

BERND RIEDERER, BSc.

Mat.No. 01430598

SCATTERING PHASES IN THE
 $H \rightarrow WW^*$ CHANNEL

MASTER'S THESIS
to achieve the university degree of
Master of Science (MSc.)
Master's degree programme: Physics

Graz University
&
Graz University of Technology

Supervisor: Univ.-Prof. Dipl.-Phys. Dr.rer.nat. Axel MAAS
Institute of Physics

Graz, February 2020

Abstract (English Version)

In standard perturbation theory massive gauge bosons, like the W- and Z-Bosons of the Electroweak interaction, are usually described by the gauge dependent elementary fields. Although they are, due to their gauge dependence, intrinsically unphysical, the results from perturbation theory agree very well with experiments. In contrast to standard perturbation theory we consider genuinely gauge invariant objects, i.e. composite states of the elementary fields, to describe the physical particles. Using a simplified lattice field theoretic description of the Electroweak-Higgs sector, we investigate the spectrum and the behavior of scattering processes in the physical scalar singlet channel. Therefore, we use a Lüscher analysis, which is commonly used in Lattice-QCD, to calculate phase shifts. These can be compared to experiment and standard perturbation theory. Due to the low amount of the used statistics, the results of this work are inconclusive. The obtained phase shifts in different parts of the phase space indicate that a resonance above the elastic threshold may still be possible in the gauge invariant description.

Abstract (Deutsche Fassung)

In Standard-Störungstheorie werden massive Eichbosonen, wie die W- und Z-Bosonen der elektroschwachen Wechselwirkung, normalerweise durch die eichabhängigen Elementarfelder beschrieben. Obwohl diese aufgrund ihrer Eichabhängigkeit inhärent unphysikalisch sind, stimmen die Ergebnisse der Störungstheorie sehr gut mit den Experimenten überein. Hier betrachten wir stattdessen echt eichinvariante Objekte, d.h. zusammengesetzte Zustände der Elementarfelder, zur Beschreibung der physikalischen Teilchen. Mit einer vereinfachten gitterfeldtheoretischen Beschreibung des Elektroschwach-Higgs-Sektors untersuchen wir das Spektrum und das Verhalten von Streuprozessen im physikalischen Skalar-Singlet-Kanal. Dazu verwenden wir eine Lüscher-Analyse, die üblicherweise in der Lattice-QCD verwendet wird, um Phasenverschiebungen zu berechnen, welche sich mit dem Experiment und der Standard-Störungstheorie vergleichen lassen. Bisher sind die Ergebnisse dieser Arbeit aufgrund des geringen Umfangs der verwendeten Statistik nicht schlüssig. Die erhaltenen Phasenverschiebungen in verschiedenen Teilen des Phasenraums deuten darauf hin, dass eine Resonanz oberhalb der elastischen Schwelle in der eichinvarianten Beschreibung noch möglich sein könnte.

Acknowledgments

Here I would like to thank a lot of people, who always helped me when I needed it the most. This work, and especially my whole studies up to now, would not have been possible without anyone of you.

First, I want to thank my advisor Prof. Axel Maas, who always answered all my questions in great detail, encouraged me (probably unconsciously) in times of slow progress and also deepened my understanding of physics very much.

I also owe a lot to the PhD students in my office, who made it a pleasure to be there. Special thanks go to Oliver Orasch, who helped me with all sorts of programming problems and other stuff, and Vincenzo Afferrante, who explained also a lot of background information for this thesis' topic to me. Apart from the PhD students, I also want to thank my friends from my earlier studies, without whom I would not be this far by now.

Furthermore, I want to thank my family who made all of this possible. Especially my parents Claudia Weselak and Thomas Riederer, who always supported me on all areas during my studies. Also I want to thank my stepfather Werner Weselak, who introduced me to the scientific/engineering world and thus sparked my interest in physics.

Finally, I want to thank my fiancée Eva Janderka simply for everything. Thank you for all your support, thank you for encouraging me to keep on working, thank you for all the time we have spent together and thank you for making my life something special. And although you do not understand a lot of this work it would not have been possible without you. I love you.

Affidavit

I declare that I have authored this thesis independently, that I have not used other than the declared sources/resources, and that I have explicitly indicated all material which has been quoted either literally or by content from the sources used. The text document uploaded to TUGRAZonline is identical to the present master's thesis.

Date

Signature

Table of Contents

Abstract	I
Acknowledgments	II
Affidavit	III
1 Introduction	1
2 SU(2)-Yang-Mills-Higgs Theory	4
2.1 Gauge Theories	4
2.2 Brout-Englert-Higgs mechanism	6
2.3 Electroweak-Higgs Sector	8
2.3.1 Perturbation theory and the FMS-mechanism	9
2.3.2 Phase diagram	12
3 Lattice Field Theory	14
3.1 Lattice Action	15
3.2 Spectroscopy	16
3.2.1 Variational Analysis	17
3.3 Lüscher Analysis	18
3.3.1 Energy Spectrum	19
3.3.2 Scattering Processes	19
4 Implementation	22
4.1 Simulation Details	22
4.2 Operators	23
4.2.1 APE smearing	23

4.2.2 Operator-Basis	24
4.3 Spectrum Extraction & Lüscher Analysis	26
4.4 Lattice Parameters	34
5 Results	36
5.1 Energy Spectra	37
5.1.1 Energy Sets	37
5.1.2 Lüscher Sets	42
5.2 Lüscher Analysis	44
6 Conclusion	48
A Generalized Zeta-function $Z_{lm}^d(r, q^2)$	50
B Statistics	53
C Vector Channel Spectra	54
Bibliography	57

Chapter 1

Introduction

In elementary particle physics we try to answer the questions “What is matter made of” and “How does it interact” at a fundamental level. The best answer so far is given by the Standard Model of Particle Physics [1], which has been verified in various experiments [2]. Though being very successful in predicting the outcome of elementary particle experiments it still has its limits. For example, a combination with gravity, described by general relativity, was not possible up to this day and there are also some discrepancies between theory and experiment like the famous $g_\mu - 2$ anomaly. These problems motivate the search for Beyond the Standard Model theories, which are expected to solve the problems while also encapsulating the Standard Model in some way.

However, to be able to find such theories it is necessary to first fully understand the Standard Model on its own. The Standard Model is a Quantum Field Theory which is invariant under some gauge symmetry. It is thus called a Gauge Theory. To investigate the theory it can be divided into separate sectors describing the three fundamental interactions: electromagnetic, strong and weak interaction. Apart from these there is one additional and very special sector in the Standard Model, the Higgs-Sector. This part contains the Higgs-Boson and the so-called Brout-Englert-Higgs mechanism [3, 4] which is needed to provide masses for the gauge bosons. Nevertheless, apart from giving masses to the bosons this also introduces some complications to the theory, which are often glossed over.

To study this problem we focus on the Electroweak-Higgs sector of the Standard Model, since this part contains the W- and Z-Bosons, the only massive gauge bosons. The fundamentals of gauge theories and especially of this sector will be

introduced in Chapter 2 of this work. As will be seen gauge theories are essentially build only from local (gauge) and global symmetries of the dynamical systems. However, if a quantity does depend on the gauge symmetry transformation it cannot be a physical observable. This will also be topic of Chapter 2.

The occurring problem is that the masses of the gauge and the Higgs bosons, as well as the gauge bosons themselves are such ‘gauge-dependent’ quantities. Thus the W- and Z-Bosons are not physical objects and should not be observable at all. But in experiments we have clear evidence that these particles indeed exist [2]. To solve this contradiction the physical objects need to be ‘gauge-invariant’, which can only be achieved by considering composite particles, i.e. bound states. This can be compared to some extent, to quantum mechanics where the gauge-dependent wave function ψ is not an observable and only the expectation value $|\psi|^2$ can be observed.

Due to the success of using gauge-dependent quantities it is necessary to find a link between the gauge-invariant composite particles, describing the physical observables, and the elementary fields which are usually used to describe particle physics phenomenology. This connection has been found by Fröhlich-Morchio-Strocchi [5, 6] already back in the 1980’s and is called gauge-invariant perturbation theory. Since then several studies [7–9] have been carried out to confirm this approach. However, apart from solving the before-mentioned problem, this approach also allows for very small deviations in some observable quantities and additional contributions in scattering processes, due to the bound state nature of the particles.

To study this behavior one needs to do non-perturbative calculations, since bound-states cannot be described by standard perturbation theory. A common method, which already has been very successful in describing Quantum-Chromodynamics (the theory of the strong interactions), is to use so-called lattice simulations. The background for this topic will therefore be introduced in Chapter 3. According to the work by Lüscher [10–13] it is possible to directly extract informations on scattering processes from these lattice simulations.

The aim of this work is to investigate the scattering processes in the physical Higgs to WW^* channel, which will be directly accessible at the HL-LHC [14]. Therefore we use genuinely gauge-invariant objects to describe the particles in a lattice formulation of the simplified Weak-Higgs sector. By doing so, we will be able to find possible deviations from standard perturbation theory, like additional

resonances or differing decay widths, which would significantly alter the search for Beyond the Standard Model Physics.

Chapter 2

SU(2)-Yang-Mills-Higgs Theory

In this chapter we will give an introduction to the basic aspects of Quantum Field Theory needed for the calculations in the following chapters. To simplify the discussion we will start by introducing Gauge Theories as well as the Brout-Englert-Higgs mechanism from a general point of view and finally combine these into a SU(2)-Yang-Mills-Higgs Theory. From this theory it will then be possible to derive the phenomenology of the (Electro-)Weak interaction in the Standard Model. For this we follow closely [15, 16].

2.1 Gauge Theories

The earliest gauge theory to be studied was (classical) electrodynamics and already from this theory it has been clear, that there exists a deep connection between symmetries and the dynamical behavior of field theories. The probably most important finding was that it is possible to directly derive the Lagrangian, which is used to describe the dynamics of field theories, from postulating a U(1) gauge invariance and requiring the equations of motion for the electrons to be the Dirac equation (see [15]). Starting from this Lagrangian the theory has then been quantized and thus led to Quantum-Electro-Dynamics (QED), which has been able to describe the electromagnetic interaction as a Quantum Field Theory. Generalizing the procedure by replacing the abelian structure of the gauge theory with a non-abelian one¹ resulted in so-called Yang-Mills theories [17] which turned out to

¹To be more precise the algebra corresponding to the gauge group needs to be a reductive, compact Lie Algebra

be the fundamental building blocks of the Standard Model.

For later reference and to clarify the conventions in this work we will now shortly present the derivation of a massless scalar Yang-Mills theory. We start by introducing some scalar fields ϕ_i and a gauge transformation $G(x)$ of these fields

$$\mathcal{L}_\phi = (\partial_\mu \phi)^\dagger (\partial^\mu \phi) \qquad \phi_i(x) \rightarrow G_{ij}(x) \phi_j(x) \qquad (1)$$

The latin indices in the equations are omitted if it is intuitively clear how they are contracted. For any Lie algebra the connection between the algebra and the group elements is given by the exponential map

$$G(x) = \exp(i\alpha^a(x)T^a) \qquad (2)$$

with $\alpha^a(x)$ some local coefficients and T^a the generators of the group in some representation. As an explicit example, for the fundamental representation of the $SU(2)$ group the generators are related to the Pauli matrices σ^a by $T^a = \frac{\sigma^a}{2}$. To keep the Lagrangian of eq. (1) invariant (gauge invariant) under this transformation it is necessary to replace the usual derivative ∂_μ by a covariant derivative

$$D_\mu = \partial_\mu - igW_\mu \qquad (3)$$

with the parameter g as the coupling constant and W_μ an additionally introduced field. This field needs to transform under the gauge group according to $W_\mu(x) \rightarrow G(x)W_\mu(x)G(x)^{-1} - \frac{i}{g}[\partial_\mu G(x)]G(x)^{-1}$ which finally makes the Lagrangian gauge invariant. Since this field is by construction a part of the algebra it can be expanded as $W_\mu = W_\mu^a T^a$, where W_μ^a are commonly known as the gauge fields. Therefore, there are always as many gauge fields as there are generators of the algebra.

To arrive at a self-consistent theory it is also necessary to include the kinetic term of the gauge fields in the Lagrangian which is described by the Yang-Mills Lagrangian

$$\mathcal{L}_{YM} = -\frac{1}{4}W_{\mu\nu}^a W^{a\mu\nu} \qquad (4)$$

$$W_{\mu\nu}^a = \partial_\mu W_\nu^a - \partial_\nu W_\mu^a + gf^{abc}W_\mu^b W_\nu^c \qquad (5)$$

with $W_{\mu\nu}^a$ being the field strength tensor and f^{abc} the structure constants of the

gauge group. The full Lagrangian for a massless scalar Yang-Mills theory reads as

$$\mathcal{L} = -\frac{1}{4}W_{\mu\nu}^a W^{a\mu\nu} + (D_\mu\phi)^\dagger(D^\mu\phi) \quad (6)$$

Before continuing with the next part, some remarks need to be made about eq. (6). First of all, the Yang-Mills Lagrangian as described in eq. (4) is not the only possible gauge invariant combination for the kinetics of the gauge fields. However, it is essentially the same as used in electrodynamics, apart from the more involved algebraic structure, and due to the great success of this theory it is a reasonable approach to use the same structure for other gauge theories as well.

Second, while the whole description here has been done without choosing a specific group or representation it turns out that the gauge fields W_μ^a always lie in the adjoint representation of the chosen algebra. That this is indeed the case can be easily seen by inserting eq. (2) into the transformation of W_μ and obtaining a relation for the gauge field transformation, which contains the covariant derivative in the adjoint representation. Also one should always keep in mind that the gauge fields are by construction gauge dependent objects which will be discussed in greater detail later on.

Finally, we are still at a classical level and therefore it makes no sense to talk about particles or the problems which occur by quantizing non-abelian gauge theories. However, to motivate the following section it is necessary to consider particles to some extent. Therefore, already with the quantization in mind (which will be dealt with in a later chapter), we will assume now that there exists a connection between the Lagrangian from above and particles observed at the laboratories.

2.2 Brout-Englert-Higgs mechanism

The ambiguity which now occurs is that the previously derived theory describes only the dynamics of massless particles, but from experiments we know that most of the particles are massive [2]. For the scalar particles ϕ_i in eq. (6) it is straight forward to introduce a mass term by adding a term which is bilinear in the fields and thus gauge invariant $\mathcal{L}_{m\phi} = -m^2\phi^\dagger\phi$ (for more details see [15]). By adding the same term for the gauge fields $\mathcal{L}_{mW} = -m^2W_\mu^{a\dagger}W^{\mu a}$, which is needed for massive gauge bosons like the W-Boson, there occurs a contradiction. Due to the more involved gauge transformation of W_μ^a compared to ϕ_i , this term breaks the gauge

symmetry and thus $\mathcal{L} \rightarrow \mathcal{L}' \neq \mathcal{L}$. Therefore, one might consider to step away from gauge theories for massive gauge bosons and try something different. By simply dropping this requirement but still keeping the same structure we arrive at an Lagrangian known as the Proca-Lagrangian. This theory however suffers from an unitarity violation problem for large energy scales [18]. This means it can only be an effective theory for a specific energy scale (e.g. the ρ -Meson in QCD).

To keep gauge invariance one needs to find a mechanism which dynamically creates the masses for the gauge fields at low energies but does not break the symmetry. One possible way of achieving this is given by the Brout-Englert-Higgs mechanism [3, 4]. Assume again the Lagrangian in eq. (6) with an additional gauge invariant potential term of the form

$$V(\phi^\dagger\phi) = -\lambda(\phi^\dagger\phi - f^2)^2 \quad (7)$$

with some parameters λ and f . This potential exhibits a minimum at $\phi^\dagger\phi = f^2$ and for a perturbative treatment of the theory, which is usually done, calculations need to be carried out near the minimum. To do so the field has to be redefined according to

$$\phi_i(x) = vn_i + h_i(x) \quad (8)$$

with $v_i = vn_i$ a constant field such that $|v| = f$ and $h(x)$ the fluctuation field satisfying $\langle h \rangle = 0$. Adding first the potential from eq. (7) to eq. (6) and inserting the split from above yields the following Lagrangian

$$\mathcal{L} = -\frac{1}{4}W_{\mu\nu}^a W^{a\mu\nu} + (D_\mu h)^\dagger (D^\mu h) + g^2 f^2 W_\mu^\dagger W^\mu - 2\lambda f^2 |h|^2 + V' \quad (9)$$

with V' collecting all additional mixing terms of h and W_μ . This potential describes the interactions between those fields and is not of interest for now. The remaining Lagrangian however shows an interesting structure which is best studied term by term. The first term remains unchanged and still describes the dynamical behavior of the gauge bosons. For the second term the scalar fields ϕ_i have been replaced by the fluctuation fields h_i which therefore become the new dynamical degrees of freedom in this theory. The final two terms are bilinear in the corresponding fields and therefore are mass terms with masses $m_W \propto gf$ for the gauge field and $m_h \propto \sqrt{\lambda}f$ for the fluctuation field.

One essential part that has been glossed over so far is what happens to the

gauge invariance. At first sight the Lagrangian now is not invariant anymore under the gauge transformation for the new scalar field $h_i(x) \rightarrow G_{ij}(x)h_j(x)$. The symmetry seems to be broken and this is usually referred to as Spontaneous Symmetry Breaking (SSB) for theories with a BEH-effect. Actually, the gauge symmetry is just hidden since this effect only occurs due to a redefinition of the fields. By using more involved transformations acting on the fields it can be seen that the symmetry is still fully intact. However, to stay in consent with the standard literature on this topic we will keep the same nomenclature, though being misleading. Additionally, it is also possible to construct the shift such that the resulting Lagrangian stays invariant under some subgroup of the original gauge group. This partial breaking is of great importance in the Standard Model to explain the massless Photon and the massive W- and Z-Bosons.

Usually, by breaking a symmetry one introduces additional massless scalar fields, depending on the number of broken group generators, to the theory known as Goldstone-Bosons [19]. At least for breaking global symmetries this is the case. However, since we are breaking a gauge symmetry these massless fields can be absorbed into the gauge fields by a gauge transformation. It is exactly this procedure of fixing the gauge such that the Goldstone fields vanish and therefore producing massive vector fields which lies at the core of the BEH-mechanism. Although not previously mentioned, gauge fixing has been implicitly done in eq. (8)² and therefore yielded massive gauge fields. One needs to keep in mind, that the occurring mass terms for the gauge fields are only due to this specific gauge fixing. In fact it is possible to construct gauges in which $|v| = 0$ and thus we would be left again with massless gauge fields. For further discussions of the BEH-mechanism and the corresponding problems, we refer to [1, 16, 20].

2.3 Electroweak-Higgs Sector

Finally we have now introduced all the necessary pieces for the Electroweak-Higgs sector of the Standard Model which is described by a $SU(2)_W \times U(1)_\gamma$ -Yang-Mills-Higgs-Theory. The $SU(2)_W$ part is responsible for the weak interaction while $U(1)_\gamma$ part describes the weak hypercharge. The BEH-mechanism breaks this group $SU(2)_W \times U(1)_\gamma \rightarrow U(1)_{em}$, which essentially describes QED with the mass-

²Note that the shift has been fixed even though $\phi_i(x) = \exp\{i\alpha^a(x)T^a\}(vn_i + h_i(x))$ would also be possible

less photon as the force carrier plus 3 massive gauge bosons mediating the weak interaction known as W^\pm - and Z-Boson and one Higgs-Boson. To study this theory in its full extent can however be very intricate and therefore we will be only considering the Weak-Higgs-Sector, leaving out the hypercharge symmetry and the already excluded Fermions. This theory differs from experiments mainly by the mass-degeneracy of all 3 gauge bosons, because the mass difference between W^\pm - and the Z-Boson is (nearly) entirely generated by QED.

The Weak-Higgs-Sector is described by a $SU(2)$ gauge theory and consists of a complex scalar doublet ϕ in the fundamental representation, which exhibits four real degrees of freedom. The gauge invariant Lagrangian is given by

$$\mathcal{L} = -\frac{1}{4}W_{\mu\nu}^a W^{a\mu\nu} + (D_\mu\phi)^\dagger(D^\mu\phi) - \lambda(\phi^\dagger\phi - f^2)^2 \quad (10)$$

with the previously used definition for the covariant derivative D_μ and the group transformations for ϕ and W_μ . Additionally to the gauge symmetry the Lagrangian also remains invariant under a global $SU(2)$ symmetry transformation acting only on the scalar field, known as the custodial symmetry. As already pointed out above, the scalar field contains four degrees of freedom and by that the free (ungauged) theory is actually invariant under the $O(4)$ symmetry. This group is isomorphic to $SU(2) \times SU(2)$ and by promoting one to a gauge group the other remains as a global symmetry. It is exactly this group which will allow us later on to arrange the physical particles in the same multiplet structures as the elementary fields in the Lagrangian and to make an identification of them.

2.3.1 Perturbation theory and the FMS-mechanism

Before carrying on the discussion to physical particles, a few words need to be said about quantizing such a theory. First of all, this theory suffers from the same difficulties as all gauge quantum field theories. When quantizing such theories using the path-integral formalism

$$\langle \mathcal{O} \rangle = \frac{1}{Z} \int \mathcal{D}\phi_i \mathcal{D}W_\mu^a e^{i \int d^4x \mathcal{L}} \mathcal{O} \quad Z = \int \mathcal{D}\phi_i \mathcal{D}W_\mu^a e^{i \int d^4x \mathcal{L}} \quad (11)$$

the integral over the gauge group usually diverges. The two possibilities of solving this problem is either fixing the gauge by a Faddeev-Popov procedure [20] or by making the integral finite by using a lattice formulation, as will be done later

in this work. In the continuum one needs to be very careful when choosing the gauge of this theory as discussed in [16]. Non-aligned gauges, like the covariant gauges, lead to a vanishing Higgs vacuum expectation value $|\langle\phi\rangle|$ (VEV) and thus massless gauge bosons. Only aligned gauges, like the 't Hooft gauges which fix the direction of the VEV, allow for non-zero gauge field masses. Second, after the quantization has been carried out, the theory is still renormalizable [21] but the renormalization scheme needs to ensure the relation $|\langle\phi\rangle| = |v| = f$ between the Higgs VEV, the constant background field and the parameter f from the Lagrangian in eq. (10). This makes the theory a well-defined QFT³ and allows us to discuss the phenomenology of the Weak-Higgs-Sector by using perturbation theory for calculating experimental accessible quantities. One example would be the phase shift in the $H \rightarrow WW^*$ channel, which will be the main interest of this work.

The problem that arises with this perturbative approach to the theory is the highly unphysical nature of the masses and the bosons themselves. That this is indeed the case, can be seen from two different perspectives. Either, it is possible to argue, that only by fixing the gauge, and thus breaking the gauge symmetry explicitly, it is possible to obtain massive bosons. However, this choice is an artificial one inserted by hand **such that** the particles are massive, although observables should not be dependent on this choice. The other argument describes the case without gauge fixing and thus is necessary for the lattice formulation of the theory. For all gauge dependent quantities, like v or W_μ^a , the expectation value in eq. (11) vanishes. This happens because a group contains for each element also the inverse one and by integrating over the whole group these cancel each other exactly. Therefore, quantities with an open gauge index cannot be physical observables and only fully contracted operators (i.e. composite states) yield non-vanishing expectation values and should be considered as physically meaningful.

In standard perturbation theory this is often ignored and the gauge dependent elementary fields of the Lagrangian are used to describe physical particles. Although, choosing the wrong starting point for the description, perturbation theory agrees strikingly well with experiments. Thus there seems to be a disagreement between a rigorous quantum field theoretic approach and the experimentally supported perturbative approach. Let us consider for instance the physical Higgs

³At least from the point of perturbation theory. For a non-perturbative treatment additional problems like the Gribov-Singer ambiguity [22, 23] arise.

particle. In standard perturbation theory the scalar field $\phi(x)$ is used for this, while a gauge-invariant operator with the same quantum numbers $J^P = 0^+$ (spin and parity) is constructed by $\phi^\dagger(x)\phi(x)$. Though being two completely different operators there is an intrinsic connection between them due to the special symmetry structure of the theory. As already mentioned the theory exhibits a $SU(2)$ gauge symmetry and a (global) $SU(2)$ custodial symmetry. This specific group structure allows to map the operators of the gauge group (gauge multiplets and custodial singlets) onto operators of the custodial groups (gauge singlets and custodial multiplets), which then yield similar results. This connection shows that there exists an exact rewriting of the physical gauge invariant states in terms of the gauge dependent states. This was originally devised by Fröhlich-Morchio-Strocchi in [5, 6] and is called the FMS mechanism. Application of the FMS-mechanism and followed by perturbation theory, which is known under the name gauge invariant perturbation theory (GIPT) [24], shows that the composite operator yields the same mass as the elementary ones to leading order. This procedure can also be carried out for the other particles in the theory, like the W-Bosons, yielding similar results. That GIPT can be used to connect rigorous quantum field theory with phenomenology has been extensively tested in several works [7–9]. Therefore, when talking about particles in this work, we always consider the gauge-invariant operators and not the elementary fields of the Lagrangian. Further, the classification by quantum numbers spin J and parity P gets an additional custodial number c and will be denoted in the form J_c^P , like 0_1^+ for the physical Higgs particle.

The aim of this work is now to study the influence of those higher order deviations from standard perturbation theory on scattering processes, especially the one in the scalar singlet channel 0_1^+ ($H \rightarrow WW^*$). Therefore, we consider several different Higgs masses to investigate the Standard Model case and also some Beyond-Standard Model theories (BSM) as well, which need additional Higgs Bosons. Also the total decay width, which is well known from perturbation theory [20], could exhibit differences and therefore would alter measurements at the experimental facilities. Additionally, the theory allows in principle for resonances in the scattering channel and could therefore alter the observable particle spectrum. This therefore needs to be investigated carefully, to correctly identify new particles at the experiments. Otherwise these could be interpreted as BSM-particles, although they are described by SM physics. This search for resonances has already been done for a different channel in [25], which showed no substantial deviations from

standard perturbation theory so far.

2.3.2 Phase diagram

Before continuing with actual calculations it is still necessary to discuss the phase diagram of the theory. The theory contains three independent free parameters: g the gauge coupling, λ the Higgs self-coupling strength and f the strength of the potential determining the Higgs vacuum expectation value v after gauge-fixing. Depending on these parameters the theory exhibits different behaviors and in fact previous lattice studies suggest that it can be divided into two regions, a QCD-like and a BEH-like one [26], though with a gauge-dependent border. The QCD-like, as the name suggests, is dominated by a QCD-like behavior and exhibits confined bound-states [27]. However, in this phase there is no BEH-effect observed and by that the ground state of the theory is in the 0_1^+ channel, corresponding to the Higgs particle. This region of the phase diagram will not be considered here, since it does not allow for a non-vanishing VEV and thus gauge invariant perturbation theory is not possible. The second region, where the ground state is in the 1_3^- vector channel, corresponding to the gauge bosons, allows for a BEH-effect and thus will be the one of interest. Though, being two different phases, it has been shown that for our specific theory the phase diagram is smoothly-connected [28] and therefore no phase transition occurs, at least for the lattice theory considered in the following chapters. This means that the phases only show quantitative different behaviors and not qualitative ones.

In the past, there have already been a lot of investigations of the phase space mostly using lattice calculations [26, 29, 30]. For this work, following [31], we will now introduce a further separation of the BEH-like domain into sections where different physics could be expected. These are classified by the ground state mass in the 0_1^+ channel according to the experimental Higgs mass $m_H \approx 125$ GeV and the W-Boson mass $m_W \approx 80.375$ GeV.

- light-Higgs region: $85 \text{ GeV} < m_{0_1^+} < 115 \text{ GeV}$
- physical-Higgs region: $115 \text{ GeV} < m_{0_1^+} < 135 \text{ GeV}$
- heavy-Higgs region: $135 \text{ GeV} < m_{0_1^+} < 155 \text{ GeV}$
- threshold region: $155 \text{ GeV} < m_{0_1^+} < 170 \text{ GeV}$

Notice that the physical-Higgs region is chosen as a 10 GeV interval around the experimental mass, due to the absence of the W-Z mass splitting and thus can also alter the Higgs mass. The two regions of interest here are the physical-Higgs region and the threshold region. For the physical region the motivation is clearly the possible comparison of the results from gauge-invariant perturbation theory with standard perturbation theory as well as with experiments, which could yield deeper insight into each approach. The threshold region is motivated from two aspects. First, for the mass of the Higgs exceeding twice the gauge boson mass there should be no stable state anymore. Standard perturbation theory suggest that there is still a resonance possible [20] but it is unclear if this is also the case for the non-perturbative approach. Second, there exist several BSM theories which suggest additional Higgs-Bosons at higher masses. If the results in this work differ from standard perturbation theory, this has direct implications on the search for those particles. For instance a much larger decay width would make the particle very hard to identify at the experiments. To study this theory in a non-perturbative way, we will switch now to the lattice formulation of the theory.

Chapter 3

Lattice Field Theory

In the previous chapter we have introduced the theory from a general point of view and motivated the need for gauge invariant and thus composite operators to describe the physical particles. However, composite operators are genuinely non-perturbative objects and therefore a suitable method is needed, which is provided by Lattice field theory. Using a lattice approach it is possible to obtain energy spectra for bound state objects and to investigate their scattering properties. Due to the smoothly connected phase diagram, as pointed out previously, it is also legit to make conclusions about the continuum behavior from the lattice calculations¹.

This chapter introduces the necessary mathematical framework for performing the lattice calculations in this work. It is however assumed that the reader is, to some extent, familiar with lattice field theory. Otherwise we refer to [32, 33] for an introduction to this topic. First, the discretized lattice action of our theory will be introduced. From the action it will be possible to extract the correlation functions and the energy spectrum for each lattice setup. This is further improved using a so-called variational analysis to obtain informations on higher energy levels, like excited states or resonances. Finally, as proposed by Lüscher in [10–13], a method to calculate the continuum energy spectrum and scattering phase shifts from differently sized lattices will be presented.

¹Of course, apart from the usual discretization artifacts and continuum limit problems, which all lattice theories exhibit.

3.1 Lattice Action

The (euclidean) lattice action of the Weak-Higgs sector can be derived by a straightforward discretization of eq. (10). However, a more stable version as outlined in [33] and already used in [31], is considered here.

$$S = \sum_{x \in \Lambda} \left[\beta \left(1 - \frac{1}{2} \sum_{\mu < \nu} \text{Re}\{\text{Tr}\{U_{\mu\nu}(x)\}\} \right) + \phi^\dagger(x)\phi(x) + \gamma(\phi^\dagger(x)\phi(x) - 1)^2 - \kappa \sum_{\mu} (\phi^\dagger(x)U_{\mu}(x)\phi(x + e_{\mu}) + \phi^\dagger(x + e_{\mu})U_{\mu}^\dagger(x)\phi(x)) \right] \quad (12)$$

with Λ the set of all lattice points for a 4-dimensional lattice with lattice spacing a and a volume $V = N^4$. Further abbreviations and relations are

$$U_{\mu\nu}(x) = U_{\mu}(x)U_{\nu}(x + e_{\mu})U_{\mu}^\dagger(x + e_{\nu})U_{\nu}^\dagger(x) \quad (13)$$

$$W_{\mu} = \frac{i}{2ag}(U_{\mu}^\dagger(x) - U_{\mu}(x)) + \mathcal{O}(a^2) \quad (14)$$

$$\beta = \frac{4}{g^2} \quad (15)$$

$$-a^2 m_0^2 = \frac{1 - 2\gamma}{\kappa} - 8 \quad (16)$$

$$\gamma = \kappa^2 \lambda \quad (17)$$

with $U_{\mu} = \exp\{igaW_{\mu}\}$ the gauge link, e_{μ} a unit vector in the μ -direction and β , κ and γ the lattice coupling parameters at the cutoff $1/a$. $m_0^2 = 2\lambda f^2$, λ and g are the bare parameters of the continuum version in eq. (10). Both the Higgs field and the gauge links are defined such that they are periodic in all directions $\Phi(x + N_{\mu}) = \Phi(x)$. Also note that the gauge links, which are the dynamical quantities in a lattice theory, are now group-valued and not algebra-valued as in the continuum. Therefore they are described by SU(2) matrices and transform under gauge transformations as

$$U_{\mu}(x) \rightarrow G(x)U_{\mu}(x)G^\dagger(x + e_{\mu}) \quad (18)$$

with $G(x)$ also SU(2) matrices as defined in eq. (2).

Choosing a physical scale for the theory is due to the phase diagram, as described above, not entirely trivial. However, in this work we will always be in-

terested in the BEH-like domain of the phase space and thus the lowest energy level has to be in the 1_3^- channel, corresponding to the physical W-Boson. Thus the scale will always be chosen such that the mass of this state is 80.375 GeV, according to the measured W-Boson mass [2]. Therefore we need to analyze the energy spectrum to find this mass.

3.2 Spectroscopy

For a spectroscopic analysis of the theory the following lattice relations are employed

$$\langle \mathcal{O} \rangle = \frac{1}{N_c} \sum_c e^{-S} \mathcal{O} \quad (19)$$

$$C(\Delta t) = \langle \mathcal{O}(t + \Delta t) \mathcal{O}^\dagger(t) \rangle = \sum_n |\langle 0 | \mathcal{O} | n \rangle|^2 e^{-E_n \Delta t} \quad (20)$$

where the first equation introduces a weighted sum over all configurations \mathcal{C} created in Monte-Carlo simulations and the second equation is used to interpret the correlator $C(\Delta t)$ in terms of energy levels E_n in lattice units. It should be mentioned that it is assumed that the expansion coefficients in eq. (20) are positive and non-vanishing. Further the correlation function has to be independent of the time step t in the expectation value because of time invariance of the theory. This can be used to improve the statistics by a factor N_t , by averaging over all time slices. Assuming the energy levels E_n to be sorted in the order $E_n \leq E_{n+1}$ it turns out, that for sufficiently large Δt , the correlator is dominated by the ground state of the theory.

$$C(\Delta t) = \sum_n |\langle 0 | \mathcal{O} | n \rangle|^2 e^{-E_n \Delta t} \stackrel{\Delta t \gg E_1^{-1}}{\approx} \text{const.} \cdot e^{-E_0 \Delta t} \quad (21)$$

So far other additional arguments of the operators \mathcal{O} have been left out intentionally. Though being possible to work in position space, it is more convenient to use momentum space and therefore a Fourier transformation needs to be applied to the operators

$$\mathcal{O}(t, \vec{\mathbf{p}}) = \sum_{x \in \Lambda} e^{i\vec{\mathbf{p}}\vec{\mathbf{x}}} \mathcal{O}(t, \vec{\mathbf{x}}) \quad (22)$$

Employing a so-called zero momentum projection $\vec{\mathbf{p}} = \vec{\mathbf{0}}$, the energy in eq. (21) becomes simply the mass M of the particle with the same quantum numbers as the operator. Thus the mass can be extracted from the exponential decay of the correlator at sufficiently large times. For small times the excited state will also contribute to the correlator and alter the exponential behavior. However, since the correlator is symmetric in time $C(\Delta t) = C(N_t - \Delta t)$ it will also deviate from the exponential form near $\Delta t = N_t/2$ and it is more reliable to replace the exponential in eq. (20) with an $\cosh(E_n(\Delta t - N_t/2))$. To make the full behavior more accessible, one introduces an effective mass, or as we will call it here an effective energy E_{eff} by

$$E_{eff}\left(\Delta t + \frac{1}{2}\right) = \ln\left(\frac{C(\Delta t)}{C(\Delta t + 1)}\right) \quad (23)$$

This effective energy usually contains a plateau somewhere in the region $0 < \Delta t < N_t/2$ which corresponds to the ground state energy E_0 . However, often one is also interested in the higher energy levels of the theory. There are several possible techniques to extract those [32] and the one we are using is called a Variational analysis.

3.2.1 Variational Analysis

For the variational analysis one exploits the fact, that on the lattice all operators with the correct quantum numbers are suitable to describe a particle. However, then this particular operator also describes all possible states in this channel and not only the one of interest. This can already be seen from the higher energy contributions in eq. (20). To avoid this problem and to disentangle the energy levels it is necessary to consider multiple operators and their cross correlations. Therefore one can introduce a correlator matrix $C_{ij}(\Delta t)$ by

$$C_{ij}(\Delta t) = \left\langle \mathcal{O}_i(t + \Delta t) \mathcal{O}_j^\dagger(t) \right\rangle = \sum_n \langle 0 | \mathcal{O}_i | n \rangle \langle n | \mathcal{O}_j^\dagger | 0 \rangle e^{-E_n \Delta t} \quad (24)$$

for a set of N operators \mathcal{O}_i , $i = 1, \dots, N$. From the right hand side it has been shown [12, 34], that diagonalizing this matrix allows to disentangle the physical

states to some extent. The eigenvalues $\lambda^{(k)}(\Delta t)$ behave as

$$\lambda^{(k)}(\Delta t) \propto e^{-E_k \Delta t} [1 + \mathcal{O}(e^{-\Delta E_k \Delta t})] \quad (25)$$

with ΔE_k the distance to next nearest energy level. To improve it even further it is possible to consider the generalized, or preconditioned, eigenvalue problem for some time step $\Delta t_0 < \Delta t$. Usually it is chosen to be 0 to perform an analyzation for all other time steps.

$$C(\Delta t)\vec{v} = \lambda C(\Delta t_0)\vec{v} \quad (26)$$

The improvement in this case is due to the suppression of higher excited states because of their larger contribution to smaller times. Also, usually the matrix values can cover several orders of magnitude and thus preconditioning makes the procedure numerically more stable by scaling all entries to similar orders of magnitude.

Concerning the operator basis used for the correlation matrix it can be said, that a larger number of interpolators improves the result in general. However, one needs to be careful, because often by increasing the basis also the statistical noise is increased and thus alters the diagonalization procedure. Hence, it is recommended to choose the operator basis such, that the overlap with the ground state is suitably large, they are linearly independent and are very close to the expected physical content of the eigenstates. Additionally, the eigenvectors \vec{v} of the problem can be used to determine which operator contributes the most to each state and by that choose the best operator basis. This will be discussed in greater detail once we have finished with the theoretical background.

3.3 Lüscher Analysis

Calculating the effective energy from eq. (23) for all obtained eigenvalues, the energy spectrum can be extracted by fitting either the plateaus to a constant or the full curve to a sum of cosh functions with different masses. Which method to choose clearly depends on several factors like the noise of the effective energy, the used lattice size and how good the disentanglement has worked. For this work we will show an example spectrum extraction in the next chapter. However, apart from obtaining the energies there is also a problem in interpreting them as infinite volume quantities. For a more general overview on the topic we recommend [35].

3.3.1 Energy Spectrum

There are mainly two problems of extracting the infinite volume energy spectrum from the lattice. The first is that due to the discretization of the theory finite volume quantities get additional corrections compared to the physical ones. To avoid this complication we will assume in the following that the lattice spacing a is small enough, such that these discretization artifacts can be neglected. The second problem appearing however is different and unavoidable. On a lattice with a finite extent N in any direction the quantum fluctuations around the particle are restricted to a small region. This restriction, and also wrap around effects on very small lattices, distort the particle and thus alters the mass. According to a work by Lüscher [10] the relation for a stable bound state of two particles of mass m behaves as

$$M_B(N) = m_B + \frac{3g^2}{16\pi m_B^2 b N} e^{-\sqrt{m^2 - \frac{m_B^2}{4}} b N} + \mathcal{O}\left(e^{-m'_B a N}\right) \quad (27)$$

with $M_B(N)$ the lattice size dependent bound state energy/mass, m_B the infinite volume quantity, g the coupling of the binding interaction, b the scattering length and m'_B the next higher state. Thus the energy levels approach the infinite volume limit exponentially fast with increasing lattice size. As already induced above, this relation only holds for stable bound states or in other words, with energies up to the elastic threshold $2m$. For resonances the extrapolation does not work as simple but it is possible to obtain other properties like the continuums phase shift δ_l or the decay width Γ .

3.3.2 Scattering Processes

The idea behind extracting scattering process informations from lattice theory can be made intuitively clear. Contrasting to the continuum, where scattering processes are always considered for particles being infinitely separated before and after the collision, this can not be assumed for the lattice since they are restricted to a box. Therefore, the particles on a lattice will always be interacting, to some extent, and by that the energy levels are distorted. From this distortion it is possible to extract informations about the binding or scattering process, since it is the same type of information. Again due to a work of Lüscher [11, 13] a connection between the lattice and the continuum has been found using perturbation theory.

The central quantity of a scattering process is the phase shift δ_l which contains all informations on the scattering of partial waves of angular momentum l . For this work, since we are only interested in the 0_1^+ channel, we have only spinless particles with vanishing center-of-mass momentum and so $l = 0$.

The interesting part of the spectrum is now the energy region between the elastic and the inelastic threshold. The elastic threshold is given by the lightest two particle scattering state in the spectrum, and the inelastic by the next higher appearing scattering state. In the case of the considered theory in eq. (12) with the parameters such that the theory is in the BEH-like domain of the phase diagram, the elastic threshold is the scattering state of two 1_3^- particles (i.e. the physical W-Boson) and the inelastic threshold is given by either four 1_3^- or two 0_1^+ particles (i.e. the physical Higgs-Boson).

Returning to the general case there will be energy levels in the region described by

$$E_n = 2\sqrt{m^2 + \vec{\mathbf{p}}_n^2} \quad (28)$$

with m the infinite-volume mass of the decay products and $\vec{\mathbf{p}}_n$ some momenta. Without any interactions these would be normal lattice momenta given by integer multiples of $2\pi/N$. However, the interaction will alter these momenta and it is instructive to define

$$\vec{\mathbf{p}}_n^2 = \left(q_n \frac{2\pi}{N}\right)^2 \quad \Rightarrow \quad q_n^2 = \left(\frac{N}{2\pi}\right)^2 \left[\left(\frac{E_n}{2}\right)^2 - m^2 \right] \quad (29)$$

with q_n usually a non-integer number, describing the deviation from the non-interacting behavior. This quantity can be determined, once the lattice size dependent energy levels E_n and the infinite volume masses m are known. From this numbers it is then possible to calculate the phase shift as pointed out in [13]. For our case the relation is given by

$$\tan(\delta_0(q_n)) = \frac{\pi^{\frac{3}{2}} q_n}{\mathcal{Z}_{00}^{\vec{\mathbf{d}}}(1, q_n^2)} \quad (30)$$

but can be generalized for other systems as is done in [36, 37]. The function $\mathcal{Z}_{lm}^{\vec{\mathbf{d}}}(r, q_n^2)$ is a purely geometric function and sometimes called a *generalized/modified Zeta* function. As the index names suggest l is the spin and m the spin projection quantum number while $\vec{\mathbf{d}}$ is connected to the center-of-mass momen-

tum of the scattering state. The function takes the form

$$\mathcal{Z}_{lm}^{\vec{d}}(r, q_n^2) = \sum_{\vec{x} \in P_{\vec{d}}} \frac{|\vec{x}|^l Y_{lm}(\vec{x})}{(\vec{x}^2 - q_n^2)^r} \quad (31)$$

$$P_{\vec{d}} = \left\{ \vec{x} \in \mathbb{R}^3 \mid \vec{x} = \vec{m} + \frac{\vec{d}}{2}, \vec{m} \in \mathbb{Z}^3 \right\}$$

with Y_{lm} the usual spherical harmonics. For $r = 1$, as used in eq. (30), the sum does not converge but can be analytically continued. Since there are several possibilities how to do this it is discussed in appendix A.

Often it is more convenient to consider the scattering width $\Gamma(s)$ or the coupling $g(s)$ as function of the center-of-mass energy $s = E_{CM}^2$. These are related to the phase shifts, for Breit-Wigner like resonances by the following formulas [36, 38]

$$\sqrt{s}\Gamma(s) \cot(\delta_l(s)) = M^2 - s \quad (32)$$

$$\frac{|\vec{\mathbf{p}}|^3}{\sqrt{s}} \cot(\delta_l(s)) = \frac{6\pi}{g(s)^2} (M^2 - s) \quad (33)$$

$$\Gamma(s) = \frac{|\vec{\mathbf{p}}|^3}{s} \frac{g(s)^2}{6\pi} \quad (34)$$

The first two equations connect the quantities directly to the phase shift and the last equation shows the connection between them. Usually the coupling constant is more of interest since it does not contain phase space effects compared to the width. Additionally, the right hand side of eq. (33) can be approximated by a linear fit $f(s) = b + cs$, with b again the scattering length already introduced in eq. (27). Thus it can be used as a consistency check of the calculations.

Chapter 4

Implementation

In the previous chapters we have introduced the motivation and the necessary mathematical tools for this work. This chapter gives the information on how the methods have been implemented and how the calculations with the corresponding error propagation have been carried out. All data for this work, if not already present, has been created by Axel Maas using the same C++ routine as in [9, 31]. Therefore, when possible, comparisons of the results have been done for validation of the analyzation procedure. The remaining analysis followed similar steps as lined out in [36, 39, 40].

4.1 Simulation Details

The creation of configurations is done in a Monte Carlo simulation (see [32] for an introduction) with different algorithms for the gauge links and the Higgs field in eq. (12). For the gauge links a combination of a heat-bath step and five over-relaxation sweeps has been used. In between each of these six gauge link updates one Metropolis sweep for the Higgs field has been performed. Therefore a Gaussian approval, tuned adaptively to a 50% acceptance probability, has been used. These 12 sweeps together constitute one single update for the field configurations. The auto-correlation of the plaquette is of the order of 1 or less such updates. Therefore, N (lattice size) such updates separate one measurement of the gauge invariant observables, to reduce the auto-correlation time. For the thermalization $2(10N + 300)$ such updates have been performed before the first measurements were done. Additionally, to reduce the noise and correlations many independent

runs have been used for the analyzation.

4.2 Operators

As already pointed out previously, it is necessary to carefully choose the operator basis for the variational analysis. The used operators should be multiplets of the custodial symmetry, which can be used to classify the physical particles, i.e. the Higgs- and W-Boson. Additionally, a procedure called smearing has been applied on the elementary fields in eq. (12) before performing measurements.

4.2.1 APE smearing

To reduce the noise of the operators it is useful to apply a technique called smearing on the fields before actual measuring the operators. There are several different possibilities of smearing the fields, but the one we are using is called APE smearing [41, 42]. Smearing can be applied multiple times to the operators and always yields new independent ones. Therefore it is possible to construct multiple operators from one field and thus can be used for a variational analysis. However, it should be mentioned that after N smearing steps, wrap around effects occur and this should be avoided. In our work a maximum of 4 smearing steps is applied before calculating the operators. The APE smearing yields for the Higgs fields and the gauge links after $n \geq 1$ smearing steps with $\alpha = 0.55$ and $d = 4$:

$$U_\mu^{(n)}(x) = \frac{1}{\sqrt{\det(R_\mu^{(n)}(x))}} R_\mu^{(n)}(x) \quad (35)$$

$$R_\mu^{(n)}(x) = \alpha U_\mu^{(n-1)}(x) + \frac{1-\alpha}{2(d-1)} \times \\ \times \sum_{\mu \neq \nu} [U_\nu^{(n-1)}(x+e_\mu) U_\mu^{(n-1)\dagger}(x+e_\nu) U_\nu^{(n-1)\dagger}(x) + \\ + U_\nu^{(n-1)\dagger}(x+e_\mu-e_\nu) U_\mu^{(n-1)\dagger}(x-e_\nu) U_\nu^{(n-1)}(x-e_\nu)] \quad (36)$$

$$\phi^{(n)}(x) = \frac{1}{1+2(d-1)} \left[\phi^{(n-1)}(x) + \right. \\ \left. + \sum_{\mu} (U_\mu^{(n-1)}(x) \phi^{(n-1)}(x+e_\mu) + U_\mu^{(n-1)}(x-e_\mu) \phi^{(n-1)}(x-e_\mu)) \right] \quad (37)$$

4.2.2 Operator-Basis

For our analysis we considered a number of basic operators in the 0_1^+ and the 1_3^- channel of the custodial symmetry [16, 31]. These local operators are

$$\mathcal{O}_H(x) = \phi^\dagger(x)\phi(x) \quad (38)$$

$$\mathcal{O}_W(x) = \text{Tr} \{ U_\mu(x) U_\nu(x + e_\mu) U_\mu^\dagger(x + e_\nu) U_\nu^\dagger(x) \} \quad (39)$$

$$\mathcal{O}_{0_n^+}(x) = \sum_{\mu=1}^3 \text{Tr} \left\{ \frac{X^\dagger(x)}{\sqrt{\det(X(x))}} U_\mu(x) \frac{X(x + e_\mu)}{\sqrt{\det(X(x + e_\mu))}} \right\} \quad (40)$$

$$\mathcal{O}_{0^+}(x) = \sum_{\mu=1}^3 \text{Tr} \{ X^\dagger(x) U_\mu(x) X(x + e_\mu) \} \quad (41)$$

$$\mathcal{O}_{1_n^-}^a(x) = \text{Tr} \left\{ \tau^a \frac{X^\dagger(x)}{\sqrt{\det(X(x))}} U_\mu(x) \frac{X(x + e_\mu)}{\sqrt{\det(X(x + e_\mu))}} \right\} \quad (42)$$

$$\mathcal{O}_{1-\mu}^a(x) = \text{Tr} \{ \tau^a X^\dagger(x) U_\mu(x) X(x + e_\mu) \} \quad (43)$$

with eqs. (38)–(41) in the 0_1^+ channel and eqs. (42)–(43) in the 1_3^- channel. They can be interpreted as the following physical objects

- \mathcal{O}_H describes the two-Higgs bound-state considered as the physical Higgs particle
- \mathcal{O}_W describes a W-ball and corresponds to the squared field strength tensor in the continuum
- $\mathcal{O}_{0_n^+}$ have no direct physical connections but yield a very stable signal [30]
- $\mathcal{O}_{1_n^-}^a$ are the vector triplets and thus are considered as the physical W-Boson

These interpretations have to be understood in the sense of an expected large overlap between the lattice operators and the physical observables. One needs to keep in mind, that all states in a channel are contributing to all operators.

From the local operators the momentum space $\mathcal{O}(\vec{\mathbf{p}})$ versions have then been obtained as described in eq. (22). From these operators we constructed the following operator basis used for the variational analysis in the 1_3^- channel

$$\mathcal{O}_{1_3^-}^{10\mu a} = \begin{cases} \mathcal{O}_{1-\mu}^{(0-4)a}(\vec{\mathbf{0}}) \\ \mathcal{O}_{1_n^-}^{(0-4)a}(\vec{\mathbf{0}}) \end{cases} \quad (44)$$

The used basis is rather small compared to the one in [31]. However, since we are only interested in the ground state mass for this channel to calculate the phase shift in the 0_1^+ channel, this is sufficient. This has been validated by comparison with previously calculated masses from a larger operator basis. For the 0_1^+ channel the basis is chosen much larger.

$$\mathcal{O}_{1-90}^{0_1^+} = \left\{ \begin{array}{l} \mathcal{O}_W^{(0-4)}(\vec{\mathbf{p}}) \\ \mathcal{O}_\rho^{(0-4)}(\vec{\mathbf{p}}) \\ \mathcal{O}_{0^+}^{(0-4)}(\vec{\mathbf{p}}) \\ \mathcal{O}_{0_n^+}^{(0-4)}(\vec{\mathbf{p}}) \\ \mathcal{O}_{1-\mu}^{(0-4)a}(-\vec{\mathbf{p}}) \mathcal{O}_{1-\mu}^{(0-4)a}(\vec{\mathbf{p}}) \\ \mathcal{O}_{1\bar{n}\mu}^{(0-4)a}(-\vec{\mathbf{p}}) \mathcal{O}_{1\bar{n}\mu}^{(0-4)a}(\vec{\mathbf{p}}) \\ \mathcal{O}_W^{(0-4)}(-\vec{\mathbf{p}}) \mathcal{O}_W^{(0-4)}(\vec{\mathbf{p}}) \\ \mathcal{O}_\rho^{(0-4)}(-\vec{\mathbf{p}}) \mathcal{O}_\rho^{(0-4)}(\vec{\mathbf{p}}) \\ \mathcal{O}_{0^+}^{(0-4)}(-\vec{\mathbf{p}}) \mathcal{O}_{0^+}^{(0-4)}(\vec{\mathbf{p}}) \\ \mathcal{O}_{0_n^+}^{(0-4)}(-\vec{\mathbf{p}}) \mathcal{O}_{0_n^+}^{(0-4)}(\vec{\mathbf{p}}) \\ \mathcal{O}_{1-\mu}^{(0-4)a}(-\vec{\mathbf{p}}) \mathcal{O}_{1-\mu}^{(0-4)a}(\vec{\mathbf{p}}) \\ \mathcal{O}_{1\bar{n}\mu}^{(0-4)a}(-\vec{\mathbf{p}}) \mathcal{O}_{1\bar{n}\mu}^{(0-4)a}(\vec{\mathbf{p}}) \end{array} \right\} \begin{array}{l} \text{such that } |\vec{\mathbf{p}}|^2 = 0 \\ \\ \\ \text{such that } |\vec{\mathbf{p}}|^2 = 1, 2 \end{array} \quad (45)$$

where the numbers $(0-4)$ in the exponents on the right hand side indicate the applied smearing steps. The different absolute momentum values need to be understood in ascending order, i.e. $\mathcal{O}_{31-60}^{0_1^+}$ corresponds to $|\vec{\mathbf{p}}|^2 = 1$. Additionally to the operators above also the two (or more) particle operators have been considered

$$\mathcal{O}_{91-180}^{0_1^+} = \left(\mathcal{O}_{1-90}^{0_1^+} \right)^2 \quad (46)$$

to find the inelastic threshold.

The first thing to notice about eqs. (44)–(46) is that the final operator basis always has zero momentum. Therefore the variational and the Lüscher analysis can be done as described in the previous chapter, without taking relative momenta into account. However, it still turns out to be useful to include the operators with back-to-back momenta in the basis, since they are reducing the noise for the non-zero momentum energy levels in the threshold region, which are the interesting ones

for the phase shifts. Also zero momentum operator means that the imaginary part should always be zero and therefore the complex conjugation in eq. (20) will not change them. That the imaginary part needs always to be zero has also been used to validate the calculations.

Second, intuitively a basis such large should be way too noisy for the variational analysis to yield reliable results. However, in our calculations it seemed to be no problem at all. Since there is no systematic approach to finding the best basis, i.e. a subset of the operators, so far, this has also been tried to achieve in this work. The first approach of simply excluding operators either showed no difference in the spectrum or it got worse. This statement however needs to be taken very carefully since of course it was not feasible to do a variational analysis for all $2^{180} - 1$ possible subsystems and compare them. Therefore only very noisy operators and those which are expected to contribute at very high energies in the spectrum, like the 4-W operators 110 to 120 and above in the basis, were excluded. Other approaches have not been tested very carefully since slightly improving the statistics yielded much better results than a rather complicated preselection.

4.3 Spectrum Extraction & Lüscher Analysis

To clarify how the calculations in this work have been done, we will present now one example calculation for the parameter set $\beta = 4$, $\kappa = 0.2708$ and $\gamma = 1$ as used in eq. (12). This case has been chosen since it exhibits all necessary steps and possible complications that occurred during calculations. Further, the statistics for this set has already been very high (See appendix B) before producing additional data for this work and thus has also been the prototype for our calculations.

Since the data for this work has been provided, we start with the operators as stated in eqs. (44)–(46). Before calculating correlation matrices one needs to remove the disconnected parts from the operators to get only the connected correlators, since otherwise a constant would be added to eq. (20). This would make the spectroscopic analysis very involved. Therefore each operator gets modified by

$$\tilde{\mathcal{O}}_i^j(t, \vec{\mathbf{p}}) = \mathcal{O}_i^j(t, \vec{\mathbf{p}}) - \langle \mathcal{O}_i(t, \vec{\mathbf{p}}) \rangle \quad \text{for } j = 1, \dots, N_C \quad (47)$$

$$\langle \mathcal{O}_i(t, \vec{\mathbf{p}}) \rangle = \frac{1}{N_C} \sum_{j=1}^{N_C} \mathcal{O}_i^j(t, \vec{\mathbf{p}}) \quad (48)$$

with i the index describing the operators in eqs. (44)–(46), j the configuration number and N_C the number of configurations used. For the operators with an open gauge and space-time index in the 1_3^- channel eq. (44) this has to be done for each index individually. However, since the expectation value eq. (48) for gauge dependent objects should vanish, as motivated earlier, the operators should stay the same. In practical calculations it turned out that the expectation value of this operators is indeed at the order of the numerical precision. For practical reasons we will now omit the tilde (\sim) on top of the operators and implicitly assume the disconnected parts to be subtracted.

For the calculation of the scattering properties the first step is to set the scale for the given parameter set. Therefore we need to know the ground state mass in the 1_3^- channel which is calculated from a variational analysis. The correlation matrix with applied time slice averaging is constructed by

$$C_{ij}^{1_3^-}(\Delta t) = \frac{1}{N_t} \sum_{t=0}^{N_t-1} \left\langle \mathcal{O}_{i\mu}^{1_3^- a}(t) \mathcal{O}_{j\mu}^{1_3^- a}(t + \Delta t) \right\rangle = \frac{1}{N_t} \sum_{t=0}^{N_t-1} C_{ij}^{1_3^-}(t, \Delta t) \quad (49)$$

with $C_{ij}^{1_3^-}(t, \Delta t)$ the correlator for the time slice t . Here the time argument $t + \Delta t$ is taken mod N_t and to reduce numerical errors also the expectation value with swapped time arguments has been averaged over. Since one configuration on its own has no physical meaning we take the time slice correlators as the stochastic variables and thus the error $\Delta C_{ij}(\Delta t)$ of the correlation matrix is just the standard error

$$\Delta C_{ij}(\Delta t) = \sqrt{\frac{1}{N_t(N_t - 1)} \sum_{t=0}^{N_t-1} [C_{ij}(t, \Delta t) - C_{ij}(\Delta t)]^2} \quad (50)$$

where the channel has been omitted since it does not make any difference and will be applied in the same way for the 0_1^+ channel later on.

To calculate the energy levels, the N_t matrices have been diagonalized with the previously described preconditioning by the first time step $C_{ij}(0)$. The eigenvalues $\lambda_i(\Delta t)$ are therefore the eigenvalues of the generalized eigenvalue problem and are always normalized to 1 for $\Delta t = 0$. To calculate the errors for the eigenvalues we also calculated the generalized eigenvalues for the matrices plus/minus the errors given in eq. (50). However, since the diagonalization of a matrix is highly non-linear it is possible that the calculated errors of the eigenvalues are smaller, larger or twisted compared to the actual eigenvalue. Therefore it is necessary to sort

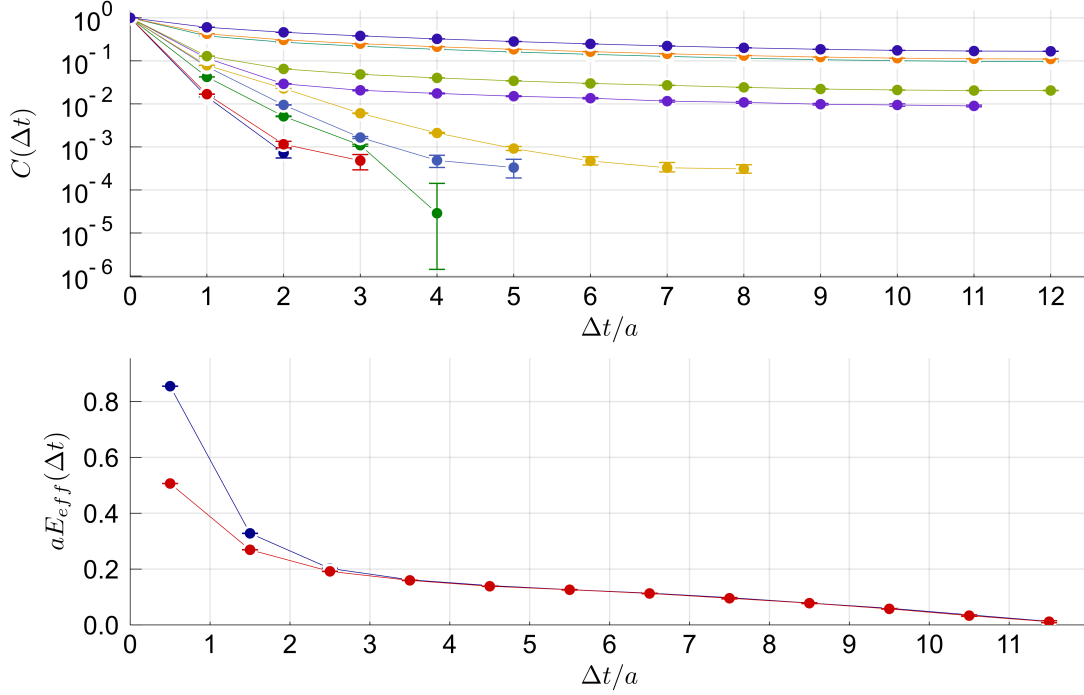


Fig. 1: Correlator (upper) and effective energy (lower) plots for $N = 24$ in the 1_3^- channel. Unphysical correlator values have been omitted. The effective energy plot contains only the two lowest energy states. See text for details.

those three possible values for each eigenvalue $\lambda_i(\Delta t)$ to get the error bounds. Before calculating the effective Energy according to eq. (23) it is useful to get rid off unphysical values for the disentangled correlators. The values are considered as unphysical if they are either smaller than 0 or not monotonically decreasing within the error bounds. That both those conditions need to be met can be easily seen from the functional form of eq. (20) which does not allow for those cases. Additionally when a value at time $\Delta t'$ is unphysical all values at larger Δt are also omitted.

After this preselection is done we can plug in the values into eq. (23) and calculate the energy levels for each lattice size N . The error of the effective energy has been calculated from error propagation and is given by

$$\Delta E_{eff}\left(\Delta t + \frac{1}{2}\right) = \frac{\Delta C(t)}{|C(t)|} + \frac{\Delta C(t+1)}{|C(t+1)|} \quad (51)$$

which in our case has to be used for each of the eigenvalues $\lambda_i(\Delta t)$ instead of $C(\Delta t)$.

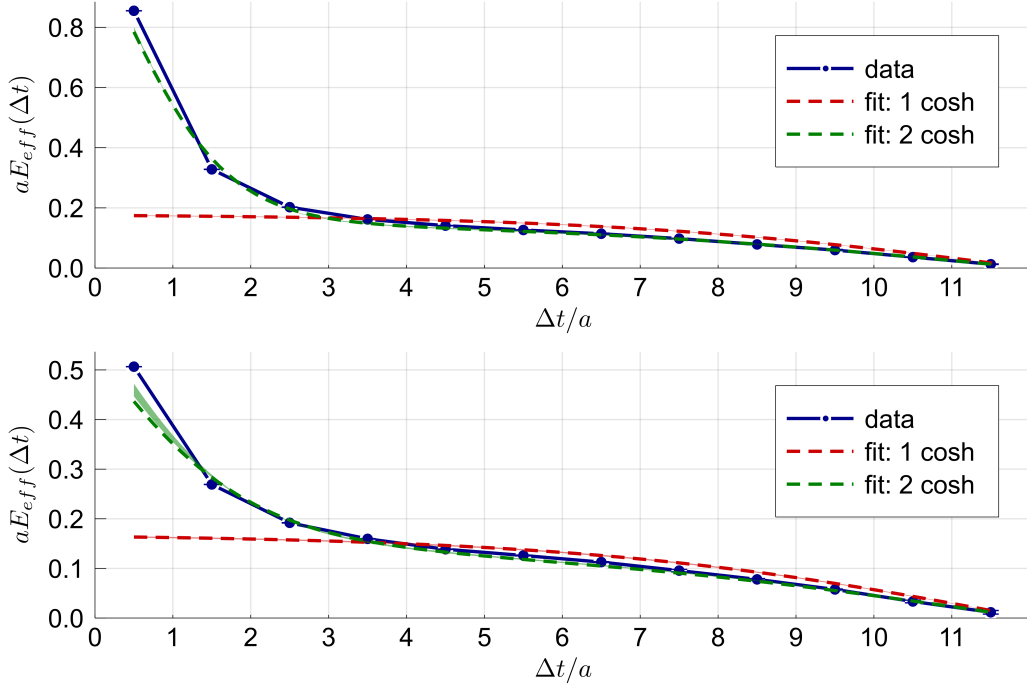


Fig. 2: Excited (upper) and ground state (lower) fits for $N = 24$ in the 1_3^- channel. Dashed lines are fits with error bounds of the fit indicated by ribbons. See text for details.

For the analysis of the ground state in this channel we always considered the two lowest effective energies as shown in fig. 1 with relative errors smaller than 50%. The reason for also taking into account the second state is because it is possible that the energy levels are crossing. To correctly identify which curve corresponds to which energy level one needs to look at the eigenvectors of the diagonalization. Usually the eigenvectors corresponding to a specific eigenvalue should not change over time. A change in the eigenvector components means that this is probably not the right eigenvalue for the energy level anymore. In this work it was sufficient to order the effective energies for each time step individually. This is probably due to the large basis which disentangles the states very well.

To extract the energy of the states the effective energies need to be fitted. Therefore the effective energy curves have been fitted by the following model function for the correlator.

$$C^{\text{fit}}(\Delta t) = A_1 \cosh\left(m_1\left(\Delta t - \frac{N_t}{2}\right)\right) + A_2 \cosh\left(m_2\left(\Delta t - \frac{N_t}{2}\right)\right) \quad (52)$$

with m_i the energies in lattice units and A_i some coefficients. This form is simply motivated by a two-state correlator as described in eq. (20), which should contain the dominant ground level and a combination of all higher contaminations. For the actual fitting process this correlator has been inserted in the effective energy formula yielding a three parameter dependent fit function, which is expected to be more reliable than fitting exponential behaviors

$$E_{eff}^{\text{fit}} = \ln \left(\frac{\cosh(m_1(t - \frac{Nt}{2})) + A'_2 \cosh(m_2(t - \frac{Nt}{2}))}{\cosh(m_1(t + 1 - \frac{Nt}{2})) + A'_2 \cosh(m_2(t + 1 - \frac{Nt}{2}))} \right) \quad (53)$$

with the coefficient A'_2 describing the relative contribution of both states.

The fitting procedure consisted of two steps. First, a simple one state fit has been performed, i.e. fixing A'_2 and m_2 to 0, to get a rough estimate of the ground state energy. To already exclude the higher state contaminations to some extent, we used a linear increasing fit weight for the data points. These have been chosen such that the first point at $\Delta t = 0.5$ had a weight of 0.1 and the last accessible point a weight of 1. The result of the first fit has then been used as a starting point to fit the two-state behavior with the same weighting. Without this preconditioning the problem is too ill-conditioned and the results would not be reliable. For almost all cases the lowest state of the two-state fit stayed close to the one of the one-state fit. The results for the two energy levels in fig. 1 are shown in fig. 2.

The errors of the fit parameters have been calculated by fitting also the upper and the lower bounds of the effective energies using the same procedure. The deviations of the fit functions for low energies in fig. 2 can be explained by only using a two-state ansatz for the correlator and by the weighting of the data points. However, for large Δt values the fitted function and the data points agree very well und thus the resulting fit parameter for the ground state is reasonable.

For the infinite volume mass this needs to be done for several different volumes. In this case we used the lattice sizes $N = \{8, 12, 16, 20, 24, 28, 32\}$. Beyond $N = 32$ computing time becomes way too large, but since the lattice mass approaches the infinite volume mass exponentially fast with the lattice size, as seen in eq. (27), it is not necessary to consider even larger lattices. Also for the largest lattice, usually the statistics were lower than for the other lattices and therefore the fit results also got larger errors as can be seen in fig. 3.

The fit function used to calculate the infinite volume mass is modeled with

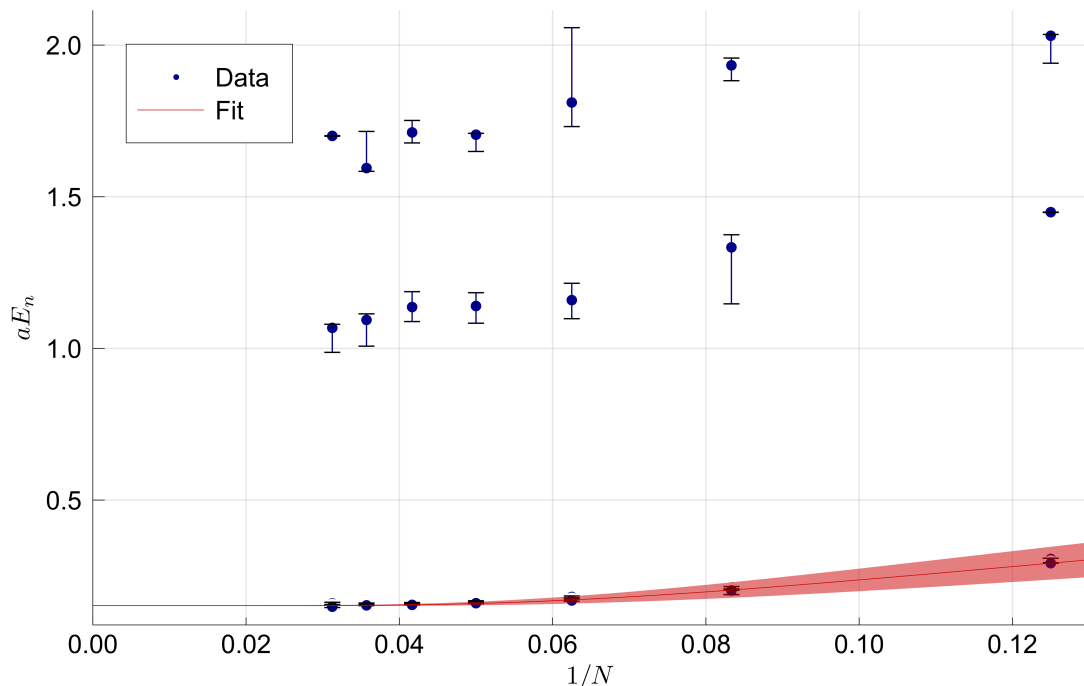


Fig. 3: Extracted energy spectrum for the 1_3^- channel over the inverse Lattice size N . For fit details see text.

respect to eq. (27)

$$E_0(N) = m_{inf} + a_1 e^{-a_2 N} \quad (54)$$

with a_i some fit parameters and m_{inf} the infinite volume mass. The errors of the fit parameters have been calculated by the fitting routine. To assure that the errors are large enough, again a weighted fit has been used, this time with the weights given by the data point errors as is usually done. However, since the errors are asymmetric the weights have been determined by the larger error of the two directions.

This results in an infinite volume mass and inverse lattice spacing for the 1_3^- channel of

$$m_{inf}^{1_3^-} = (0.152 \pm 0.002) a^{-1} \stackrel{!}{=} 80.375 \text{ GeV} \quad \Rightarrow \quad a^{-1} = 528 \text{ GeV} \quad (55)$$

which sets the scale of this theory (see table 1 in the following chapter for comparison).

For the scattering phase shift in the 0_1^+ the same procedure needs to be repeated

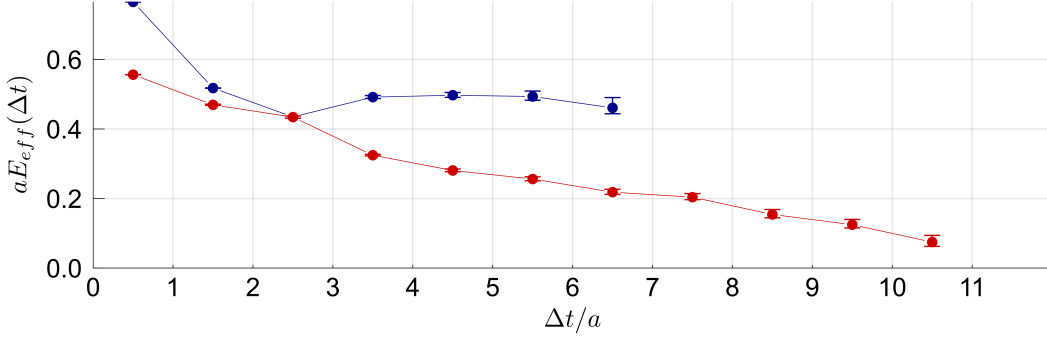


Fig. 4: Effective energy plot for $N = 24$ in the 0_1^+ channel. Unphysical energy values have been omitted. The effective energy plot contains only the two lowest energy states. The correlator plot has been omitted, since it does not give any additional informations. See text for details.

for a different correlation matrix. The full matrix is given by

$$C_{ij}^{0_1^+}(\Delta t) = \frac{1}{N_t} \sum_{t=0}^{N_t-1} \langle \mathcal{O}_i^{0_1^+}(t) \mathcal{O}_j^{0_1^+}(t + \Delta t) \rangle = \frac{1}{N_t} \sum_{t=0}^{N_t-1} C_{ij}^{0_1^+}(t, \Delta t) \quad (56)$$

which is a symmetric matrix of size 180×180 and the operators are again the connected ones (see eq. (47)). In this channel the before mentioned energy level crossing occurs more often than in the 1_3^- channel. However, most of the times the eigenvectors were too noisy to make a clear statement on the energy levels.

In fig. 4 it can be already seen, that it is not clear if the energy level identification has been done correct for $\Delta t \geq 2$. Since we are mainly interested at the region where Δt is large the point at $\Delta t = 2.5$ has been ignored for the fits of both energy levels in fig. 5.

Combining the results from the 1_3^- channel with the spectrum in the 0_1^+ yields the following ground state mass as obtained from fig. 6

$$m_{inf}^{0_1^+} = (0.2244 \pm 0.0006) \text{ a}^{-1} = (118.5 \pm 0.4) \text{ GeV} \quad (57)$$

Thus the infinite volume mass in the scalar singlet channel lies in the physical-Higgs region.

The resulting spectrum of the scalar singlet channel in fig. 6 shows qualitatively good agreement with the expected spectrum. For large lattices, i.e. farther left on the plot, the statistics have not been good enough for the fit routine to yield a

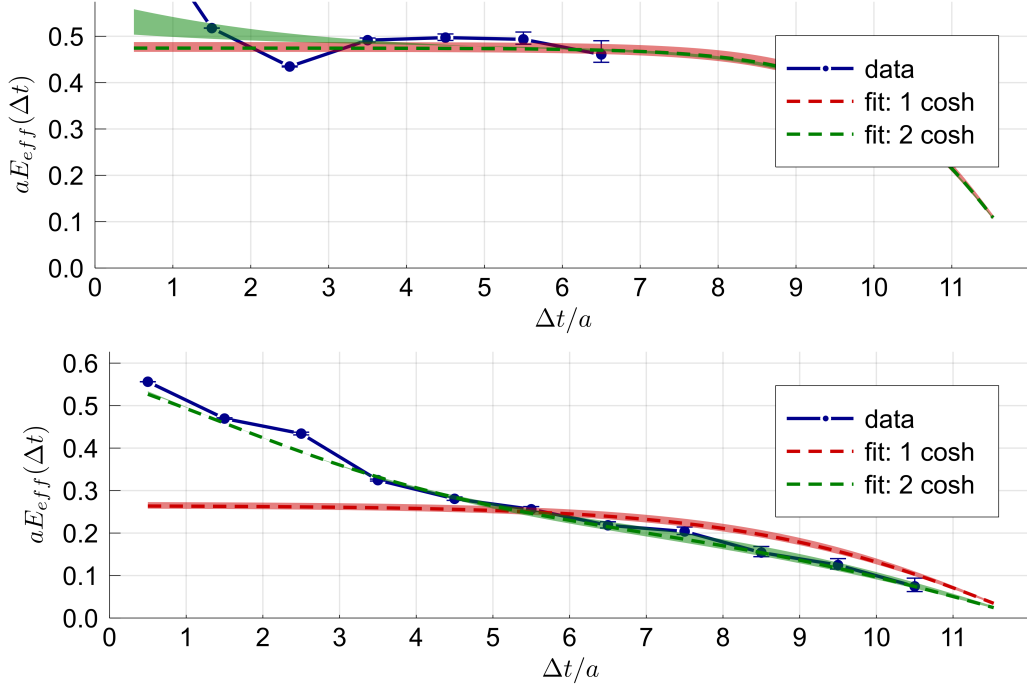


Fig. 5: Excited (upper) and ground state (lower) fits for $N = 24$ in the 0_1^+ channel. Dashed lines are fits with error bounds of the fit indicated by ribbons. See text for details.

conclusive separation of the ground state and the first scattering state. However, for the smallest lattice the value is in perfect agreement with the expectation. Also the two-particle bound state, giving the inelastic threshold, is identifiable by naive state counting. It also seems, that depending on the lattice size, the first state above the ground state to be found is either the elastic or the inelastic threshold. For the intermediate lattice sizes the ground state and the scattering state are very close and could not be separately identified. This should be however possible to overcome by improving statistics or the fitting routine. The points above the inelastic threshold are not of much interest for this work, but it is encouraging to see them agree with the expected spectrum in most parts.

The problem with this data set, while being a perfect prototype for the energy spectrum extraction, is that there is no significant data point in the threshold region and thus a phase shift analysis is not possible. Also the naive finite momentum states already left the threshold region before the point $N = 32$, which should give some points in the region if it were flatter. Therefore, it is necessary to consider different parameter sets for a phase shift analysis.

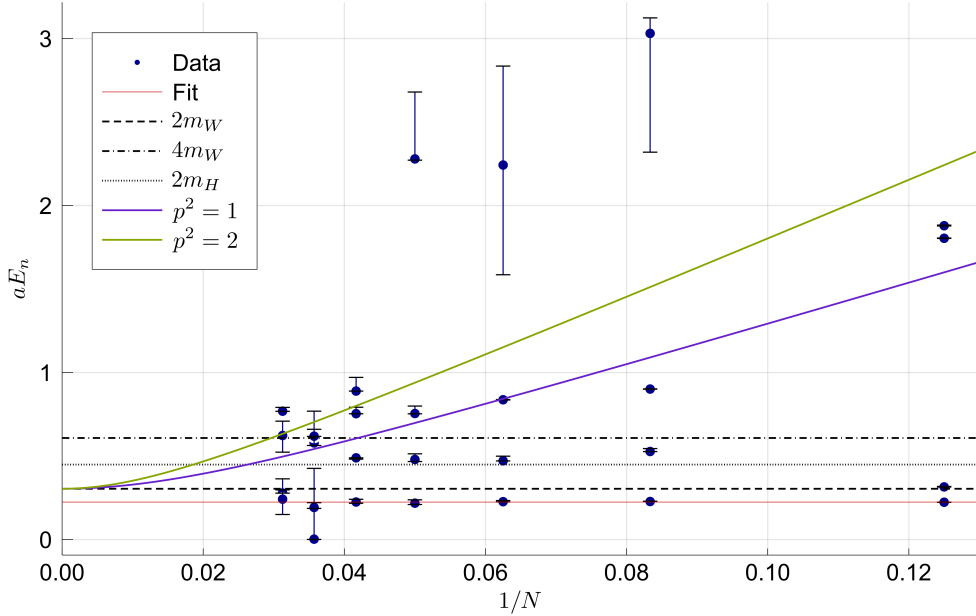


Fig. 6: Extracted energy spectrum for the 0_1^+ channel over the inverse Lattice size N . For fit details see text. Also the elastic threshold (black dashed), the inelastic threshold (lower on of black dotted or dashed-dotted) and the two lowest finite momentum scattering states (green and blue solid) have been added.

4.4 Lattice Parameters

Choosing the right parameter set for the analysis is a very important task and needs to be carefully done. For this work we wanted the parameter sets to fulfill several purposes and had to choose them such that

1. the theory is in the BEH-like domain, i.e. the ground state is in the 1_3^- channel
2. the ground state of the 0_1^+ channel can be classified as either a Higgs in the light-, physical- and threshold-region of the phase diagram
3. there are at least some energy levels in the threshold region for our lattice sizes

In fact the third point is the most important, but it is not directly predictable. The idea therefore is to choose a suitable lattice spacing in a way that the finite momentum states stay below the inelastic threshold up to the values reachable with the affordable lattice sizes. To still assure the point two one needs to fix the

ratio of the groundstate masses in the vector and the scalar channel and then find a maximum lattice spacing. The upper bounds which have been found for the lattice spacings in the different Higgs-regions are given by

- light-Higgs region: $a^{-1} \lesssim 150 \text{ GeV}$
- physical-Higgs region: $a^{-1} \lesssim 350 \text{ GeV}$
- heavy-Higgs region: $a^{-1} \lesssim 450 \text{ GeV}$
- threshold-Higgs region: $a^{-1} \lesssim 500 \text{ GeV}$

where it has been used that at least the first finite momentum state has a minimum of two points (for the $L = \{32, 28\}$ lattices) in the threshold region.

With the knowledge of this upper bounds for the lattice spacing and previous phase space studies of the theory [31] it was possible to find parameters satisfying all three criteria from above. These parameter sets have been analyzed as described above and used for a phase shift analysis.

Chapter 5

Results

This chapter combines the findings of this work in the separate phase space regions as described in the introductory chapters. The analyzed parameter sets have been chosen as described previously and are listed in table 1 below. The used statistics are listed in appendix B.

Tab. 1: Analyzed Parameter Sets

Set Name	Region	β	κ	γ	$\alpha_{200 \text{ GeV}}$	$a^{-1} \setminus \text{GeV}$	N
Example	physical	4.0000	0.2708	1.000	0.119	505	8:4:32
Energy 1	threshold	3.8000	0.2679	1.000	0.153	620	8:8:32
Energy 2	light	2.7984	0.2927	1.343	0.664	471	8:8:32
Energy 3	physical	2.7984	0.2927	1.317	0.605	453	8:4:32
Energy 4	threshold	3.8000	0.2736	1.000	0.128	448	8:8:32
Energy 5	threshold	3.4258	0.2922	1.380	0.157	395	8:8:32
Energy 6	threshold	2.7984	0.2954	1.239	0.492	323	8:8:32
Energy 7	physical	2.4964	0.2939	1.036	0.718	271	8:8:32
Lüscher 1	threshold	2.7984	0.2984	1.317	0.492	323	8:8:32
Lüscher 2	threshold	2.8859	0.2981	1.334	0.448	322	8:8:32
Lüscher 3	physical	4.0000	0.2850	0.970	0.219	309	8:4:32
Lüscher 4	physical	4.0000	0.3000	1.000	0.211	255	8:4:32

The parameters in the table are the expected phase space region, the lattice parameters β , κ and γ , the weak coupling $\alpha_{200 \text{ GeV}}$ at the given minimal momentum, the inverse lattice spacing a^{-1} from the 1_3^- ground state masses and the used lattice sizes written in the form $N_l : N_s : N_u = \{ N = N_l + nN_s \mid n \in \mathbb{N}^0 \wedge N \leq N_u \}$. The values for a^{-1} , $\alpha_{200 \text{ GeV}}$ and the expected region are the results of previous investigations [31]. These can differ from the results shown here due to the different

operator basis. However, the inverse lattice spacing should always be roughly the same. Therefore the parameter sets are divided into two categories: *Lüscher* and *Energy*. For those named *Lüscher* it has been possible to do a phase shift analysis, while those named *Energy* do not contain data points in the threshold region. This will be discussed for each case individually. Also it should be noted that the sets do not follow a line of constant physics, which is already intended to be seen by the different regions they are describing.

For each parameter set the spectra in the 1_3^- and the 0_1^+ channel have been calculated as explicitly shown in the previous chapter for the set *Example*. Since there is no Lüscher analysis possible this set will not be resumed here. For the other sets it is then straightforward to calculate the phase shift in the scalar singlet channel by plugging all data points from the threshold region into eq. (29) and subsequently into eq. (30). For an error estimation of the phase shift the error bounds of the energy levels in the threshold regions have also been used separately to calculate phase shifts. This gives a rough estimate of the error region but still leaves place for improvement (using for instance a Bootstrap method).

5.1 Energy Spectra

5.1.1 Energy Sets

For the parameter sets in the *Energy* part of table 1 we obtained the masses in the 1_3^- and the 0_1^+ channel as listed below

Tab. 2: Mass results for the *Energy* parameter sets

Set Name	$am_{1_3^-}$	$am_{0_1^+}$	$m_H \setminus \text{GeV}$	$a^{-1} \setminus \text{GeV}$	Region
Energy 1	0.114 ± 0.003	0.200 ± 0.002	141 ± 1	705	heavy
Energy 2	0.151 ± 0.007	0.17 ± 0.06	91 ± 32	532	light
Energy 3	0.171 ± 0.003	0.228 ± 0.001	107 ± 1	470	light
Energy 4	0.177 ± 0.002	0.243 ± 0.001	110 ± 1	454	light
Energy 5	0.199 ± 0.004	0.287 ± 0.007	116 ± 3	404	physical
Energy 6	0.244 ± 0.006	0.29 ± 0.02	95 ± 7	329	light
Energy 7	0.286 ± 0.010	0.336 ± 0.003	95 ± 1	281	light

Comparing table 1 and table 2 we see that for all sets the mass in scalar singlet channel became lower and thus falls into another region. Therefore also no phase

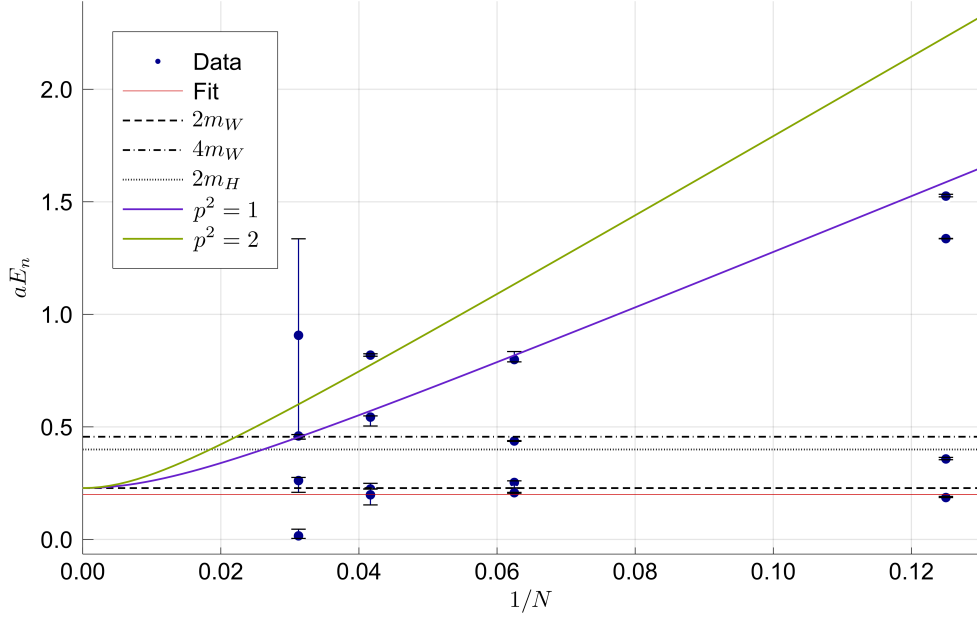


Fig. 7: Parameter Set: *Energy1*. Extracted energy spectrum for the 0_1^+ channel over the inverse Lattice size N . Also the elastic threshold (black dashed), the inelastic threshold (lower on of black dotted or dashed-dotted) and the two lowest finite momentum scattering states (green and blue solid) have been added.

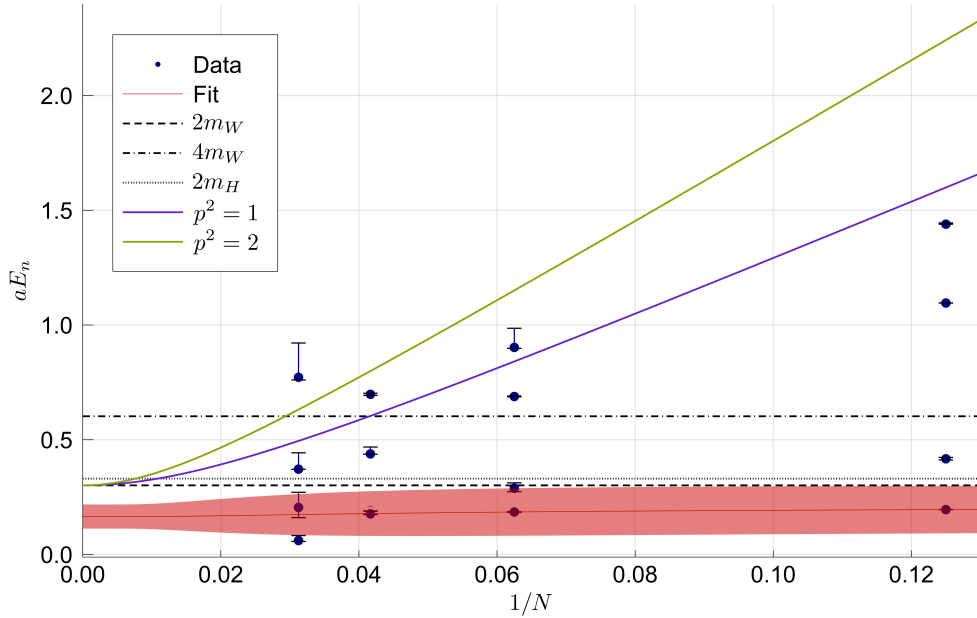


Fig. 8: Parameter Set: *Energy2*. Extracted energy spectrum for the 0_1^+ channel over the inverse Lattice size N . Also the elastic threshold (black dashed), the inelastic threshold (lower on of black dotted or dashed-dotted) and the two lowest finite momentum scattering states (green and blue solid) have been added.

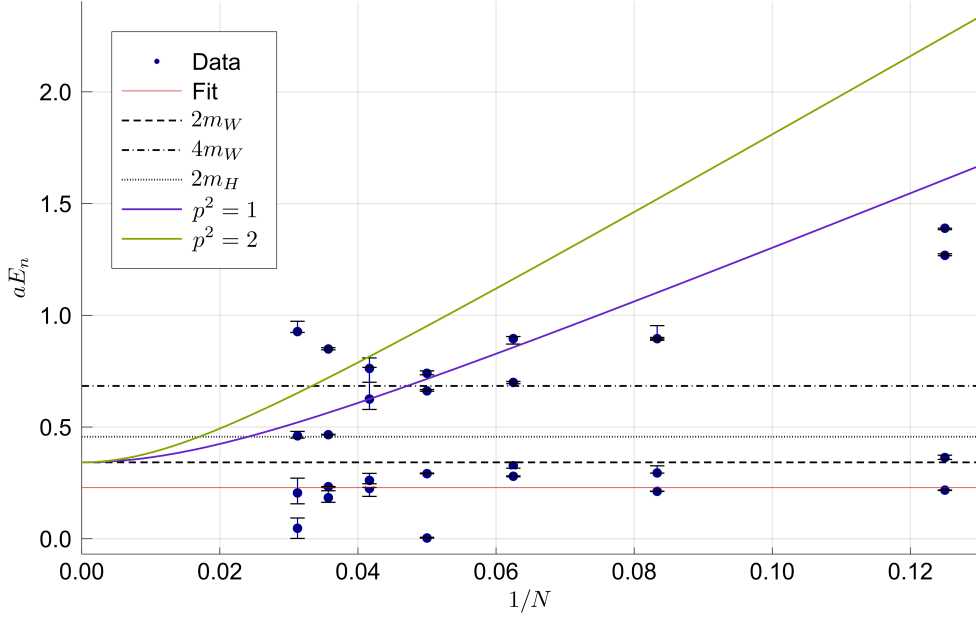


Fig. 9: Parameter Set: *Energy3*. Extracted energy spectrum for the 0_1^+ channel over the inverse Lattice size N . Also the elastic threshold (black dashed), the inelastic threshold (lower on of black dotted or dashed-dotted) and the two lowest finite momentum scattering states (green and blue solid) have been added.

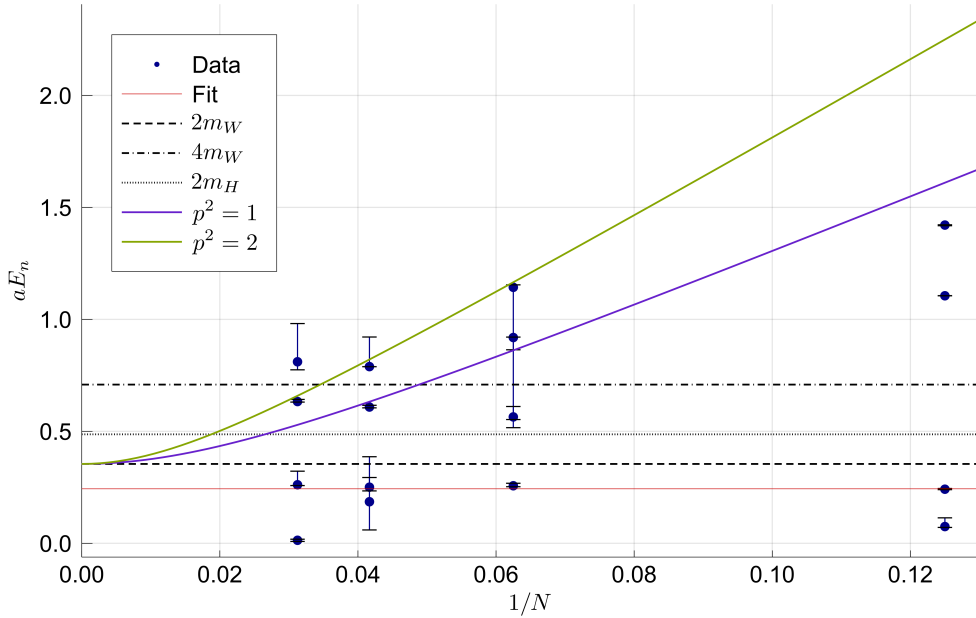


Fig. 10: Parameter Set: *Energy4*. Extracted energy spectrum for the 0_1^+ channel over the inverse Lattice size N . Also the elastic threshold (black dashed), the inelastic threshold (lower on of black dotted or dashed-dotted) and the two lowest finite momentum scattering states (green and blue solid) have been added.

shift analysis is possible since the inverse lattice spacings are too large for the newly found regions. Except for the sets *Energy1* and *Energy2* the lattice spacings are less than 10 % of the given values in table 1 and are usually within the range of the error for the mass. The reasons for the large differences in the phase space regions for the parameter sets can be various. First, the regions given in table 1 have been obtained only from the $L = 24$ lattice and no infinite volume extrapolation has been done. However, as can be seen in figs. 7–13 the fits are very flat and thus this should not alter the results to this extent. In the vector triplet channel these fits are not always flat. This explains the large difference in the inverse lattice spacing for *Energy1* and *Energy2* since the scale is also set by the vector triplet mass on the $L = 24$ lattice. The spectra and the fits of these sets are shown in appendix C. Second, for the calculation of the ground state mass there has only a very small operator subset been used (see [31]). Therefore the large basis used in this work, disentangles the energy levels much more and thus the fitting has less higher order contaminations, which explains that the mass becomes lower. Third, it has to be noted, that probably the errors of the infinite volume extrapolations are underestimated. This is the result of the weighted fit, which reduces the impact of data points with large errors on the fit. However, by that also the calculated error is less effected by those points and thus results in a small uncertainty region. This can be seen in figs. 7–13, since the fit error does not always cover the error bounds of all data points. Finally, also the low statistics and few lattice sizes used for these parameter sets (compared to the *Lüscher* sets) alters the whole spectrum. We chose to not improve the statistics for a further analyzation of these spectra, since according to these results no phase shift analysis would be possible.

What also needs to be discussed are the outliers in figs. 7–13 which are located close to zero energy. All of them have been excluded from the ground state fits because of their unphysical nature. These low energy points are always due to one of two reasons. For low energy points and small lattices, i.e. $L = \{8, 12\}$ in fig. 10 and fig. 11, there were too few points for a reliable three parameter fit as shown in eq. (53). Therefore, the fit procedure effectively turns it into a one parameter problem by setting one energy level close to zero. The other low energy points for larger lattices, i.e. $L = \{20, 24, 32\}$ in figs. 7–11, are due to a similar problem though of different origin. For these lattices the statistics were not good enough for the fitting routine to find a sufficient solution for three parameters. Also in this case one energy in the fit function is tuned to small energies and effectively

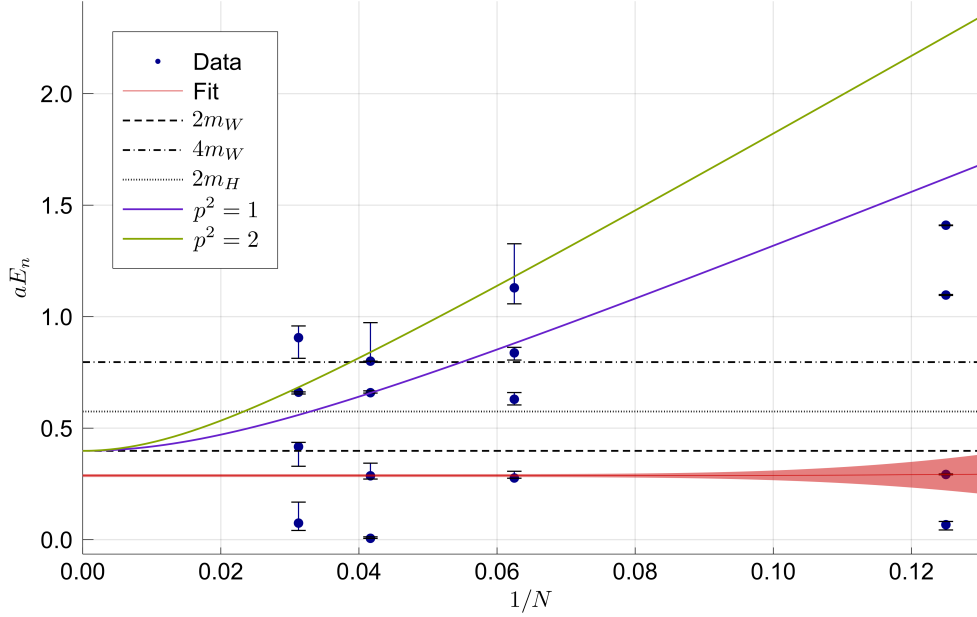


Fig. 11: Parameter Set: *Energy5*. Extracted energy spectrum for the 0_1^+ channel over the inverse Lattice size N . Also the elastic threshold (black dashed), the inelastic threshold (lower on of black dotted or dashed-dotted) and the two lowest finite momentum scattering states (green and blue solid) have been added.

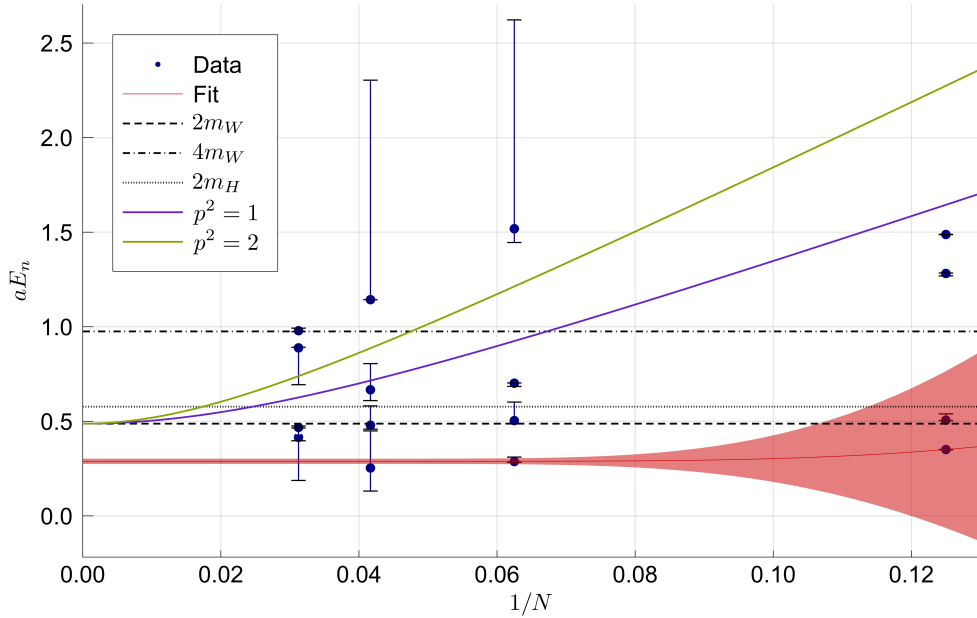


Fig. 12: Parameter Set: *Energy6*. Extracted energy spectrum for the 0_1^+ channel over the inverse Lattice size N . Also the elastic threshold (black dashed), the inelastic threshold (lower on of black dotted or dashed-dotted) and the two lowest finite momentum scattering states (green and blue solid) have been added.

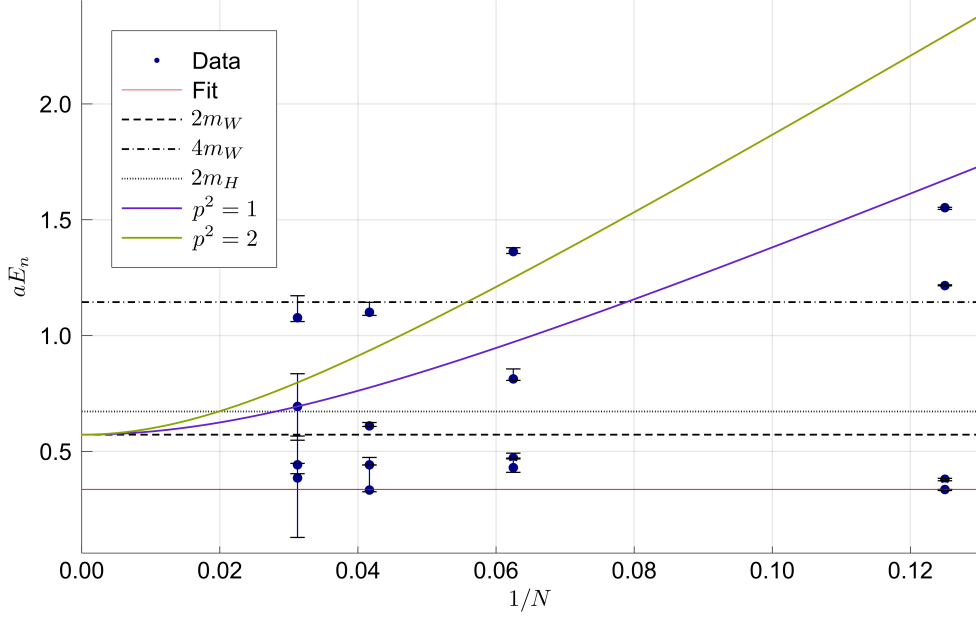


Fig. 13: Parameter Set: *Energy7*. Extracted energy spectrum for the 0_1^+ channel over the inverse Lattice size N . Also the elastic threshold (black dashed), the inelastic threshold (lower on of black dotted or dashed-dotted) and the two lowest finite momentum scattering states (green and blue solid) have been added.

only one parameter is being fitted. Additionally this is being complicated by the already mentioned energy level mixing. This usually became relevant for larger lattices with low statistics and therefore only very few points in the effective energy plots were usable for the fits. Summing it up, all low energy points are numerical artifacts and do not correspond to low energy levels in this work and thus all these parameter sets lie in the BEH-like domain of the phase space.

5.1.2 Lüscher Sets

For the parameter sets in the *Lüscher* part of table 1 we obtained the masses in the 1_3^- and the 0_1^+ channel as listed below

Tab. 3: Mass results for the *Lüscher* parameter sets

Set Name	$am_{1_3^-}$	$am_{0_1^+}$	$m_H \setminus \text{GeV}$	$a^{-1} \setminus \text{GeV}$	Region
Lüscher 1	0.245 ± 0.004	0.276 ± 0.010	91 ± 4	328	light
Lüscher 2	0.245 ± 0.003	0.314 ± 0.007	103 ± 3	328	light
Lüscher 3	0.254 ± 0.001	0.372 ± 0.005	118 ± 2	317	physical
Lüscher 4	0.311 ± 0.002	0.503 ± 0.001	130 ± 1	259	physical

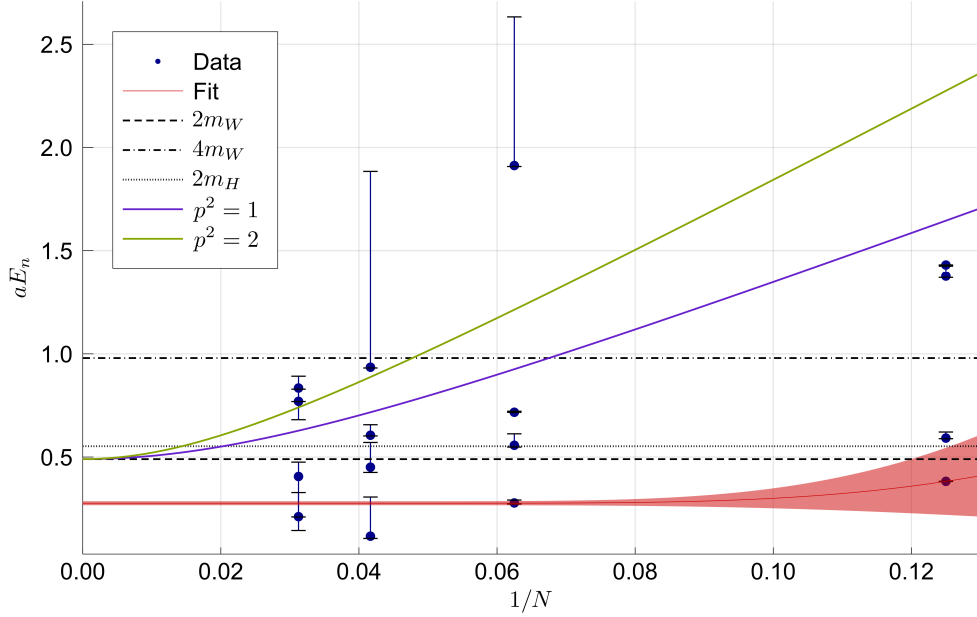


Fig. 14: Parameter Set: *Lüscher1*. Extracted energy spectrum for the 0_1^+ channel over the inverse Lattice size N . Also the elastic threshold (black dashed), the inelastic threshold (lower on of black dotted or dashed-dotted) and the two lowest finite momentum scattering states (green and blue solid) have been added.

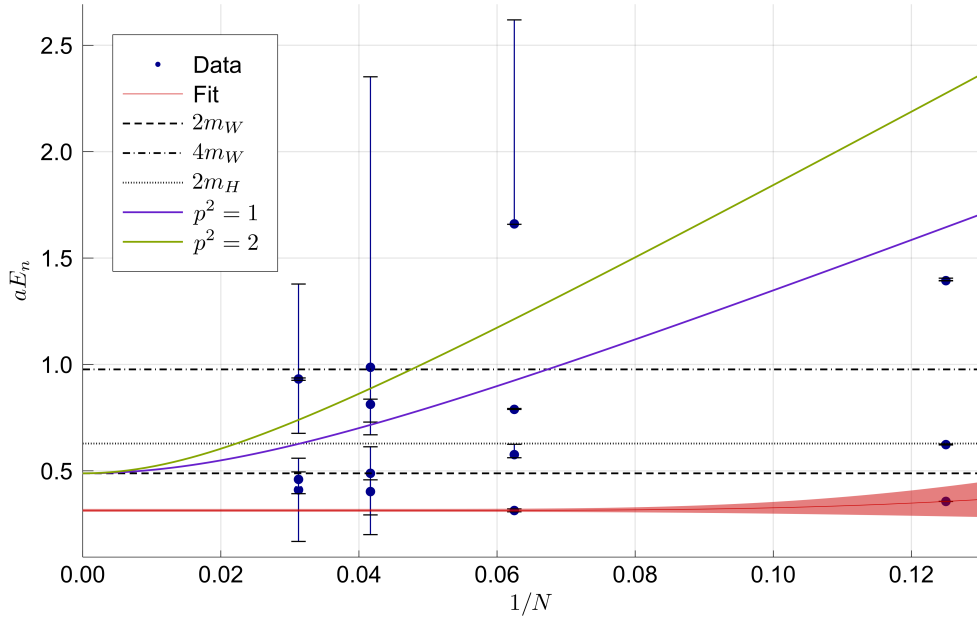


Fig. 15: Parameter Set: *Lüscher2*. Extracted energy spectrum for the 0_1^+ channel over the inverse Lattice size N . Also the elastic threshold (black dashed), the inelastic threshold (lower on of black dotted or dashed-dotted) and the two lowest finite momentum scattering states (green and blue solid) have been added.

For this parameter sets all the inverse lattice spacings are in perfect agreement with the ones in table 1. In this case the ground state in the vector channel showed almost now deviation for the $L = 24$ lattice compared to the infinite volume mass and thus the lattice spacings agree. Also again some regions differ from the previously found ones, but since the inverse lattice spacings are small enough, it is still possible to do the phase shift analysis. In figs. 14–17 we see that for all data sets the finite momentum states leave the threshold region after reaching the accessible area of our lattice sizes.

Again the same considerations from the previous section concerning the masses apply here. One additional problem occurring for these sets is that for the larger lattices it becomes more difficult to separate the ground state and the first scattering state (i.e. the elastic threshold) in the fits. This is best seen in figs. 16 and 17, where the data points are tending towards the threshold for larger lattices. However, this effect does not alter the calculation of the infinite volume mass significantly since due to their larger errors they give a smaller contribution to the fits. To reduce this effect, it would be necessary to increase statistics and also consider more than only the two lowest energy states for fitting, as described in the previous chapter. However, in these cases the the third state has been too noisy for fitting and thus has not been done.

5.2 Lüscher Analysis

From the data points in figs. 14–17 in the threshold region it is now possible to obtain the phase shift information using eq. (29) and eq. (30). The generalized zeta function has been evaluated as described in appendix A.

The resulting phase shift for the different parameter sets are shown in fig. 18. In all figures the energy axis is limited to the threshold region, because outside of this region the Lüscher analysis does not work. Therefore some error bars are leaving the plot pane if the energy level also leaves the elastic region. For instance compare fig. 16, where two error bars cross the elastic threshold, with fig. 18c. The error bars on the y-axis are a bit more involved. Due to the periodic behavior of the tan-function in eq. (30) it is not possible to have phase shifts larger than π or smaller than 0. This periodicity has to be reflected onto the error bars. Therefore, a value whose errorbar exceeds π by Δe is also compatible with being in the range $[0, \Delta e]$. This periodic condition has also been implemented in fig. 18.

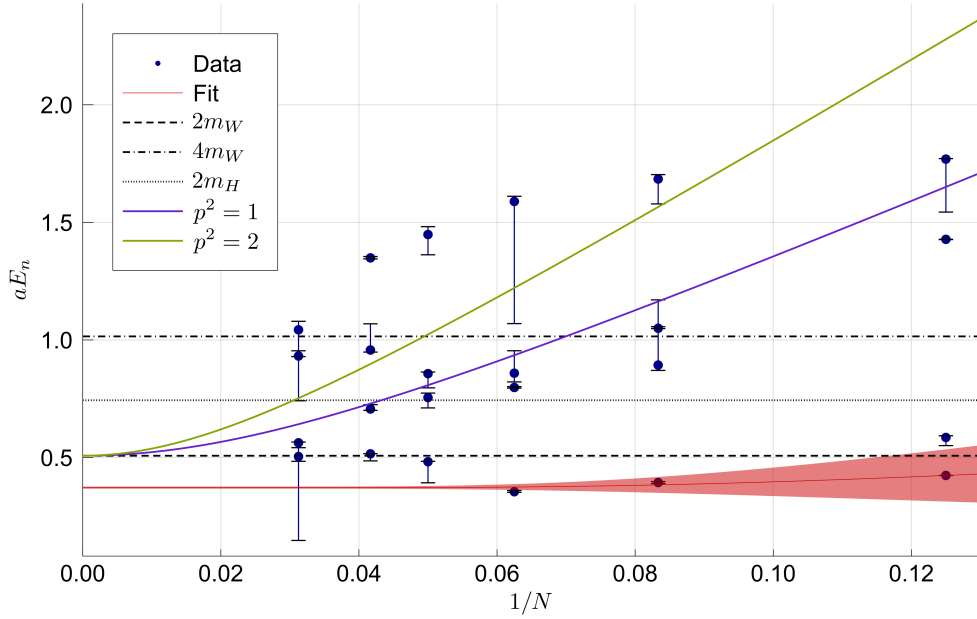


Fig. 16: Parameter Set: *Lüscher3*. Extracted energy spectrum for the 0_1^+ channel over the inverse Lattice size N . Also the elastic threshold (black dashed), the inelastic threshold (lower on of black dotted or dashed-dotted) and the two lowest finite momentum scattering states (green and blue solid) have been added.

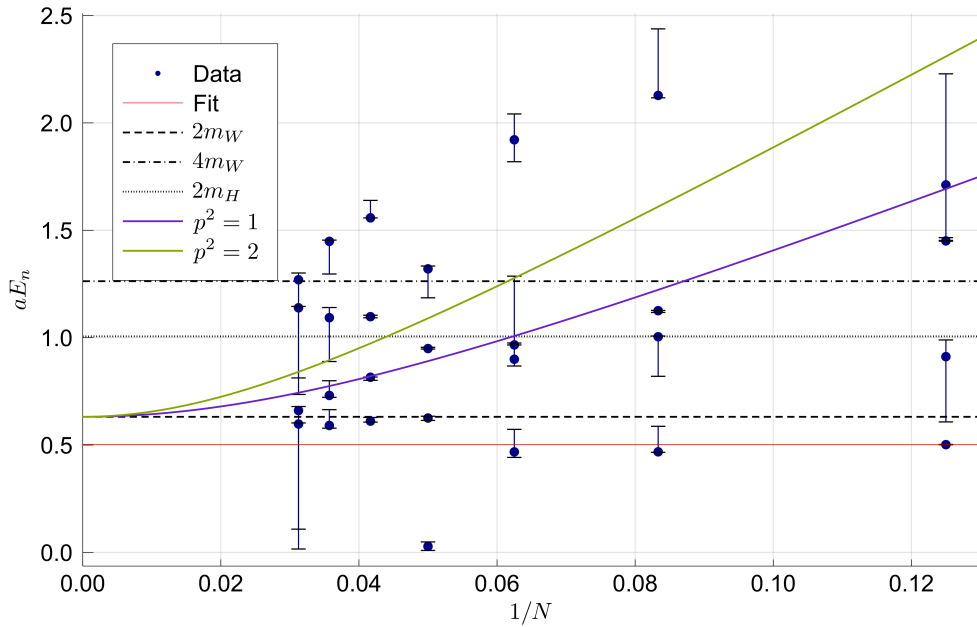


Fig. 17: Parameter Set: *Lüscher4*. Extracted energy spectrum for the 0_1^+ channel over the inverse Lattice size N . Also the elastic threshold (black dashed), the inelastic threshold (lower on of black dotted or dashed-dotted) and the two lowest finite momentum scattering states (green and blue solid) have been added.

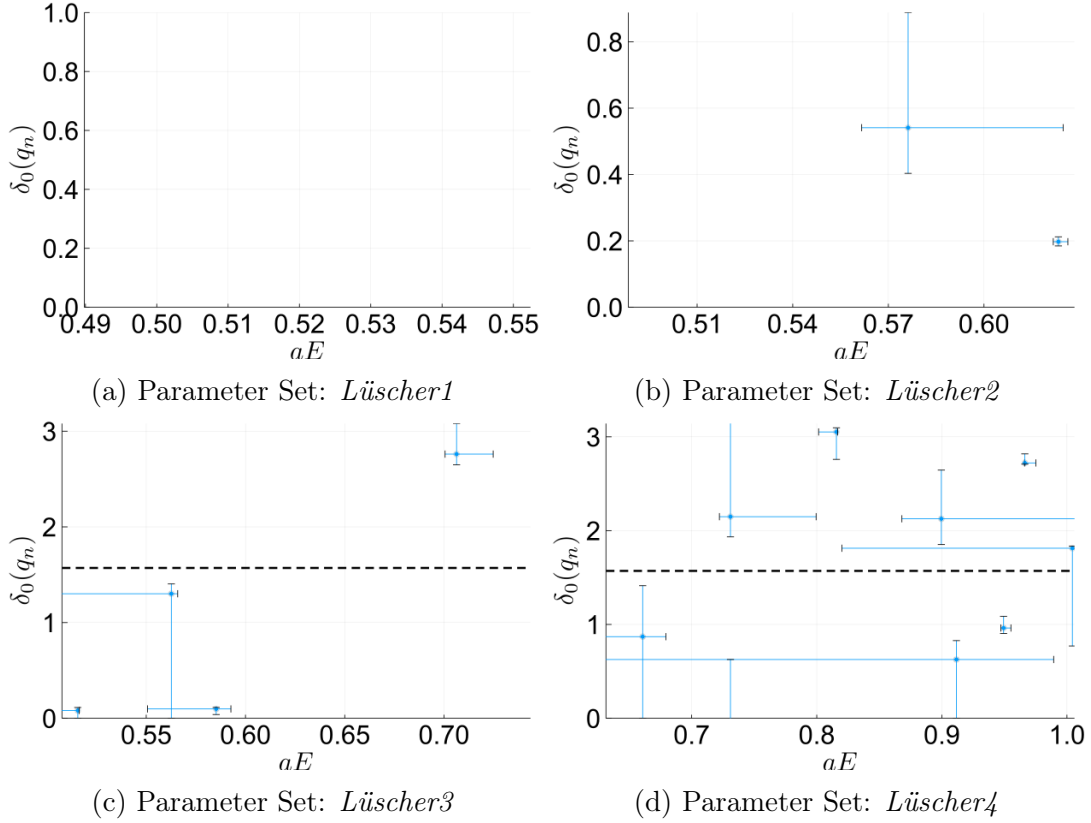


Fig. 18: Phase shifts in rad for the given parameter sets in the 0_1^+ channel over the Energy in lattice units. The x-axis is limited to the threshold region while the y-axis is periodic in π . For details see text. The black dashed line indicates a phase shift value of $\pi/2$.

In fact there is no point in the threshold region for *Lüscher1* and thus no points in fig. 18a. However, currently higher statistics are produced and it is expected to yield some points in this region.

For *Luescher2*, as shown in fig. 18b, there are only two points which are not very reliable due to the large errors. Though, it seems that the phase shift is not crossing $\pi/2$ and thus no resonance is found for this parameter set.

The last two parameter sets *Lüscher3* and *Lüscher4* are quite different. Although again the error bars are relatively large, there are points above $\pi/2$. For *Lüscher3* in fig. 18c there is one point in the upper part of the plot and the error bars are not compatible with values below $\pi/2$. To verify that this point is indeed in the error range more statistics is needed. However, without some points in the intermediate energy range of the threshold region it is not possible to exactly calculate the position and the width of the resonance without very large

uncertainties.

In the *Lüscher4* case there are enough points in the interesting region and also one very stable point is located near $\pi/2$ which should make it possible to locate the position of the resonance very clear. To verify that this is indeed a resonance it is necessary to clarify the phase shift values of the other points in the threshold region. Since they are all compatible with values above and below $\pi/2$ it is not possible to make a conclusive statement about the location and width of the possible resonance.

Since, all datasets are inconclusive with the current amount of statistics it is also not possible to do the fits for the coupling and decay width as stated in eq. (33) and eq. (34). However, with improved statistics these sets could exhibit a resonance for a physical-Higgs (*Lüscher3* and *Lüscher4*), while *Lüscher2* also seems to be a parameter near to the physical-Higgs region where no resonance occurs.

Chapter 6

Conclusion

In this thesis we have investigated the energy spectrum of a SU(2)-Yang-Mills-Higgs theory in the scalar singlet channel for various phase space points. Therefore we considered genuinely gauge-invariant operators in the scalar singlet 0_1^+ and the vector triplet 1_3^- channel of the custodial symmetry, where the groundstate represents the physical Higgs-Boson and W-Bosons of the Electroweak interaction respectively. This has been done by using a variational analysis for suitably large operator bases in both channels as shown in section 4.2.2.

The obtained groundstate masses in the vector triplet channel were all in agreement with previous studies in [31] as can be seen table 2 and table 3. This shows that using a much a smaller basis than the one in [31] is already sufficient, if one is only interested in the ground state, as expected. Additionally, also for most parameter sets it is not necessary to do the infinite volume extrapolation for the mass, since in most cases the masses on the largest lattices coincided with the infinite volume quantities. Nevertheless, this should always be checked and the finite volume mass has to be considered only as a rough estimate of.

In the scalar singlet channel the groundstate masses differed from previous investigations and always got smaller as can be seen by comparing the phase space regions in table 1 with table 2 and table 3. This is mainly due to two reasons. First, in this work we used a very large operator basis in this channel. Therefore the effective energy curves contains less contaminations from higher energy levels and thus gets flatter. By that the masses can be extracted more stable and are usually smaller than the ones obtained from smaller operator bases. Second, we also have used in this channel an infinite volume extrapolation for the masses

and thus the infinite volume mass is smaller or equal to the mass obtained on the largest lattice. Again we want to point out, that all regions and masses in previous investigations have been obtained from the $N = 24$ lattice.

For some parameter sets it has been possible to do a Lüscher analysis as is shown in section 5.1.2 and to obtain phase shift values (see fig. 18) in the elastic region of the energy spectrum. The results from these calculations are inconclusive by now, since the error bars do not permit to clearly identify the behavior. However, from the present amount of statistics it seems that a resonance above the elastic threshold is possible for the investigated theory. This is indicated by the phaseshift crossing the value $\pi/2$ in fig. 18c and fig. 18d. To verify that this is indeed the case further investigations need to be carried out.

To sum it up, we have shown in this work that the obtained energy spectrum in the scalar singlet channel of the SU(2)-Yang-Mills-Higgs theory for gauge-invariant composite operators (i.e. custodial multiplets) coincides with the spectrum from standard perturbation theory. By simple state counting there appeared no additional stable states in the spectrum. However, the results of this work also suggest that it is possible to find resonances above the elastic threshold.

For future computations on this work, it would be necessary to first improve statistics for the cases where a Lüscher analysis has been possible. Additionally also the error estimation could be improved by applying some sort of Bootstrap methods. This may already be sufficient to reduce the uncertainties in the phase shift values. For the cases where resonances appear the next step would be to repeat these calculations along lines of constant physics. From these results one can calculate the mass, the width and the coupling of the resonance as pointed out in section 3.3.2. These possible resonances need to be studied very carefully, since otherwise if they show up in experiments they could be falsely identified as non-standard-model particles.

Appendix A

Generalized Zeta-function $\mathcal{Z}_{lm}^{\vec{d}}(r, q^2)$

Here we want to present the analytical continuation and numerical evaluation of the zeta function $\mathcal{Z}_{lm}^{\vec{d}}(r, q^2)$ defined in eq. (31). This has already been discussed by Lüscher in [11, 13] and on several other occasions [37, 43] for different system, i.e. moving reference frames. However, we follow here [44], where a faster converging version is presented. Additionally, it turned out that the final formula given in [44] for the $l = m = 0$ and $\vec{d} = \vec{0}$ case includes a typographical error. Therefore, we will present now the derivation of a numerically stable, analytically continued zeta function in the rest frame for the case of spinless particles, following [44]. For comparison we will also state the final, slower converging formula derived in [37].

The definition of the zeta function $\mathcal{Z}_{00}^{\vec{d}}(r, q^2)$ is

$$\mathcal{Z}_{00}^{\vec{d}}(r, q_n^2) = \frac{1}{\sqrt{4\pi}} \sum_{\vec{x} \in P_{\vec{d}}} \frac{1}{(\vec{x}^2 - q_n^2)^r} \quad (58)$$

$$P_{\vec{d}} = \left\{ \vec{x} \in \mathbb{R}^3 \left| \vec{x} = \vec{m} + \frac{\vec{d}}{2}, \vec{m} \in \mathbb{Z}^3 \right. \right\}$$

and takes on finite values for $\text{Re}\{r\} > 3/2$. For the scattering phase shift formula in eq. (30) we need $r = 1$ and thus an analytic continuation. First we split the sum into two parts

$$\sum_{\vec{x}} \frac{1}{(\vec{x}^2 - q_n^2)^r} = \sum_{\vec{x}^2 < q_n^2} \frac{1}{(\vec{x}^2 - q_n^2)^r} + \sum_{\vec{x}^2 > q_n^2} \frac{1}{(\vec{x}^2 - q_n^2)^r} \quad (59)$$

with $\vec{x} \in P_{\vec{d}}$. For the second sum, the denominator is always larger zero and thus

it is possible to rewrite it in the following way

$$\begin{aligned}
 \sum_{\vec{x}^2 > q_n^2} \frac{1}{(\vec{x}^2 - q_n^2)^r} &= \sum_{\vec{x}^2 > q_n^2} \frac{1}{\Gamma(r)} \int_0^\infty \frac{dt}{(\vec{x}^2 - q_n^2)} \left(\frac{t}{\vec{x}^2 - q_n^2} \right)^{r-1} e^{-t} = \\
 &= \frac{1}{\Gamma(r)} \sum_{\vec{x}^2 > q_n^2} \int_0^\infty du u^{r-1} e^{-u(\vec{x}^2 - q_n^2)} = \\
 &= \frac{1}{\Gamma(r)} \sum_{\vec{x}^2 > q_n^2} \left[\int_0^1 du u^{r-1} e^{-u(\vec{x}^2 - q_n^2)} + \int_1^\infty du u^{r-1} e^{-u(\vec{x}^2 - q_n^2)} \right] = \\
 &= \frac{1}{\Gamma(r)} \int_0^1 du u^{r-1} e^{uq_n^2} \sum_{\vec{x}^2} e^{-u\vec{x}^2} - \sum_{\vec{x}^2 < q_n^2} \frac{1}{(\vec{x}^2 - q_n^2)^r} + \sum_{j=1}^r \frac{1}{(s-j)!}
 \end{aligned} \tag{60}$$

where the second term in the last line exactly cancels the first term in eq. (59). For the first term we can use Poisson's summation formula

$$\sum_{\vec{n} \in \mathbb{Z}^3} f(\vec{n}) = \sum_{\vec{n} \in \mathbb{Z}^3} \int d^3r f(\vec{r}) e^{i2\pi\vec{n}\vec{r}} \tag{61}$$

and by integrating over \vec{r} and explicitly inserting \vec{x} from eq. (58) we arrive at

$$\frac{1}{\Gamma(r)} \int_0^1 du u^{r-1} e^{uq_n^2} \sum_{\vec{x}^2} e^{-u\vec{x}^2} = \frac{1}{\Gamma(r)} \int_0^1 du u^{r-1} e^{uq_n^2} \left(\frac{\pi}{u} \right)^{\frac{3}{2}} \sum_{\vec{m} \in \mathbb{Z}^3} (-1)^{\vec{m}\vec{d}} e^{-\frac{\pi^2 \vec{m}^2}{u}} \tag{62}$$

The divergence at $r = 1$ is due to the $\vec{m} = \vec{0}$ term in the sum. Splitting the sum in a divergent and a finite part finally allows us to separate the divergence and to analytically continue the function

$$\int_0^1 du u^{r-1} e^{uq_n^2} \left(\frac{\pi}{u} \right)^{\frac{3}{2}} = \pi^{\frac{3}{2}} \sum_{k=0}^{\infty} \frac{(q_n^2)^k}{k!} \int_0^1 du u^{r-\frac{3}{2}+k-1} = \pi^{\frac{3}{2}} \sum_{k=0}^{\infty} \frac{(q_n^2)^k}{k!} \frac{1}{r+k-3/2} \tag{63}$$

which only works for $r > 3/2$. However, the right hand side takes a finite value for $r = 1$ and thus can be used for continuation. The final expression for the zeta

function for $r = 1$ is

$$\begin{aligned} \sqrt{4\pi} \mathcal{Z}_{00}^{\vec{\mathbf{d}}}(r, q_n^2) &= \sum_{\vec{\mathbf{x}}^2} \frac{e^{-(\vec{\mathbf{x}}^2 - q_n^2)}}{(\vec{\mathbf{x}}^2 - q_n^2)} + \pi^{\frac{3}{2}} \sum_{k=0}^{\infty} \frac{(q_n^2)^k}{k!} \frac{1}{k - 1/2} + \\ &+ \int_0^1 du e^{uq_n^2} \left(\frac{\pi}{u}\right)^{\frac{3}{2}} \sum'_{\vec{\mathbf{m}} \in \mathbb{Z}^3} (-1)^{\vec{\mathbf{m}} \cdot \vec{\mathbf{d}}} e^{-\frac{\pi^2 \vec{\mathbf{m}}^2}{u}} \end{aligned} \quad (64)$$

The first term here is due to the heat kernel regularization used to make the sum convergent by analytical continuation. The summation $\sum'_{\vec{\mathbf{m}} \in \mathbb{Z}^3}$ intends that $\vec{\mathbf{m}} = \vec{\mathbf{0}}$ has been left out.

Inserting also $\vec{\mathbf{d}} = \vec{\mathbf{0}}$ into the formula yields finally a numerically stable fast converging representation of the generalized zeta function as needed in eq. (30).

$$\begin{aligned} \sqrt{4\pi} \mathcal{Z}_{00}^{\vec{\mathbf{d}}}(r, q_n^2) &= \sum_{\vec{\mathbf{m}} \in \mathbb{Z}^3} \frac{e^{-(\vec{\mathbf{m}}^2 - q_n^2)}}{(\vec{\mathbf{m}}^2 - q_n^2)} + \pi^{\frac{3}{2}} \sum_{k=0}^{\infty} \frac{(q_n^2)^k}{k!} \frac{1}{k - 1/2} + \\ &+ \int_0^1 du e^{uq_n^2} \left(\frac{\pi}{u}\right)^{\frac{3}{2}} \sum'_{\vec{\mathbf{m}} \in \mathbb{Z}^3} e^{-\frac{\pi^2 \vec{\mathbf{m}}^2}{u}} \end{aligned} \quad (65)$$

Note, that here the first sum **does include** $\vec{\mathbf{m}} = \vec{\mathbf{0}}$ not as stated in [44]. That this is indeed the correct form can be seen by comparison with [37, 43].

The implementation used in this work follows eq. (65) and has been verified by comparison with values obtained as described in [37]. In this paper a different expression for eq. (63) is given by

$$\int_0^1 du u^{r-1} e^{uq_n^2} \left(\frac{\pi}{u}\right)^{\frac{3}{2}} = -2\pi^{\frac{3}{2}} + \int_0^1 du \left(e^{uq_n^2} - 1\right) \left(\frac{\pi}{u}\right)^{\frac{3}{2}} \quad (66)$$

and both yielded numerically the same results but the integral version converged much slower. Additionally the zeros of the generalized zeta function have been compared with those stated in [39] and they agreed.

Appendix B

Statistics

In the following table the used amount of statistics for each parameter set according to table 1 is shown. The measurement of one configuration has always been separated as described in section 4.1. For *Lüscher3* the datasets for $N = 28$ have been corrupted and could not be used for the analyzation.

Tab. 4: Number of used configurations for the Parameter Sets

N	8	12	16	20	24	28	32
Example	95616	85558	81270	86760	172104	79638	12118
Energy 1	95616	-	81270	-	14325	-	11027
Energy 2	122160	-	119168	-	144053	-	17595
Energy 3	107488	121344	106848	91200	220837	87570	14425
Energy 4	123152	-	119840	-	43375	-	15798
Energy 5	92364	-	82390	-	131803	-	17339
Energy 6	81360	-	74140	-	98156	-	16745
Energy 7	162305	-	159400	-	93543	-	29331
Lüscher 1	137265	-	127990	-	121872	-	19665
Lüscher 2	208274	-	149740	-	107923	-	18343
Lüscher 3	291968	86460	259489	130640	199023	-	19772
Lüscher 4	464912	147122	238648	167890	232215	109667	29749

Appendix C

Vector Channel Spectra

In this appendix we present the additional calculated energy spectra in the 1_3^- channel for the data sets with large discrepancies compared to previous studies. The parameter sets are named as stated in table 1.

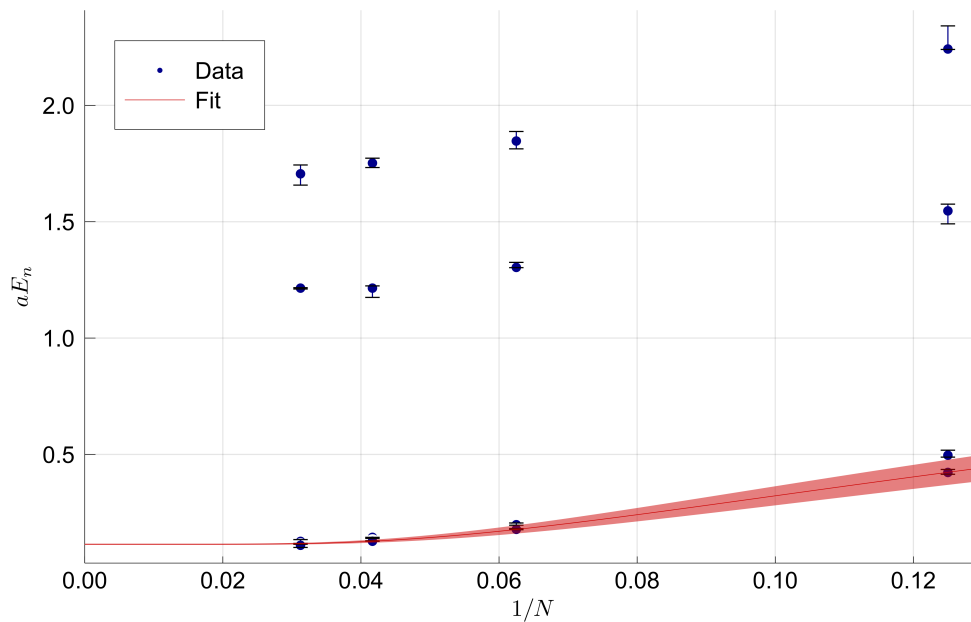


Fig. 19: Parameter Set: *Energy1*. Extracted energy spectrum for the 1_3^- channel over the inverse Lattice size N .

In fig. 19 we see, that the energy levels show a strong volume dependency and therefore the masses at the used lattices differ from the infinite volume mass. The

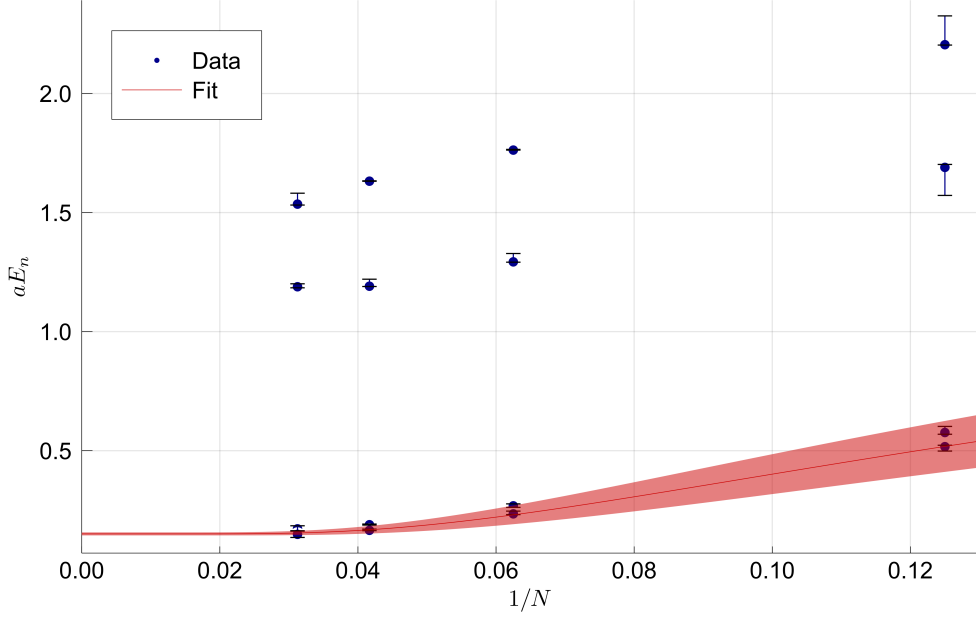


Fig. 20: Parameter Set: *Energy2*. Extracted energy spectrum for the 1_3^- channel over the inverse Lattice size N .

full fit results according to eq. (54) for this parameter set are

$$m_{inf} = 0.114 \pm 0.003 \quad a_1 = 1.504_{-0.13}^{+0.14} \quad a_2 = 0.197_{-0.009}^{+0.010} \quad (67)$$

which yields for $L = 24$

$$M(L = 24) = (0.1273_{-0.007}^{+0.008}) a^{-1} \quad \Rightarrow \quad a^{-1} = 631 \text{ GeV} \quad (68)$$

and would set the scale. This inverse lattice spacing is again in perfect agreement with table 1 and explains the discrepancy in table 2 for the set *Energy1*.

In fig. 20 we see, that the energy levels show also a strong volume dependency and therefore the masses at the used lattices differ again from the infinite volume mass. The full fit results according to eq. (54) for this parameter set are

$$m_{inf} = 0.151 \pm 0.007 \quad a_1 = 1.69 \pm 0.23 \quad a_2 = 0.19 \pm 0.02 \quad (69)$$

which yields for $L = 24$

$$M(L = 24) = (0.17 \pm 0.02) a^{-1} \quad \Rightarrow \quad a^{-1} = 472 \text{ GeV} \quad (70)$$

and would set the scale. This inverse lattice spacing is again in perfect agreement with table 1 and explains the discrepancy in table 2 for the set *Energy2*.

Bibliography

- [1] D. Griffiths. *Introduction to elementary particles*. Wiley-VCH, 2008.
- [2] M. Tanabashi et al. Review of particle physics. *Phys. Rev. D*, 98, 3, 2018.
- [3] F. Englert et al. Broken Symmetry and the Mass of Gauge Vector Mesons. *Phys. Rev. Lett.*, 13:321–323, 1964.
- [4] P. W. Higgs. Broken Symmetries and the Masses of Gauge Bosons. *Phys. Rev. Lett.*, 13:508–509, 1964.
- [5] J. Fröhlich et al. HIGGS PHENOMENON WITHOUT A SYMMETRY BREAKING ORDER PARAMETER. *Phys. Lett.*, 97B:249–252, 1980.
- [6] J. Fröhlich et al. HIGGS PHENOMENON WITHOUT SYMMETRY BREAKING ORDER PARAMETER. *Nucl. Phys.*, B190:553–582, 1981.
- [7] A. Maas. Accessing directly the properties of fundamental scalars in the confinement and Higgs phase. *Eur. Phys. J.*, C71:1548, 2011. arXiv: 1007.0729 [hep-lat].
- [8] A. Maas. Bound-state/elementary-particle duality in the Higgs sector and the case for an excited 'Higgs' within the standard model. *Mod. Phys. Lett.*, A28:1350103, 2013. arXiv: 1205.6625 [hep-lat].
- [9] A. Maas et al. Two- and three-point functions in Landau gauge Yang-Mills-Higgs theory. *JHEP*, 04:006, 2014. arXiv: 1312.4873 [hep-lat].
- [10] M. Lüscher. Volume Dependence of the Energy Spectrum in Massive Quantum Field Theories. 1. Stable Particle States. *Commun. Math. Phys.*, 104:177, 1986.
- [11] M. Lüscher. Volume Dependence of the Energy Spectrum in Massive Quantum Field Theories. 2. Scattering States. *Commun. Math. Phys.*, 105:153–188, 1986.

-
- [12] M. Lüscher et al. How to Calculate the Elastic Scattering Matrix in Two-dimensional Quantum Field Theories by Numerical Simulation. *Nucl. Phys.*, B339:222–252, 1990.
- [13] M. Lüscher. Two particle states on a torus and their relation to the scattering matrix. *Nucl. Phys.*, B354:531–578, 1991.
- [14] G. Apollinari et al. High Luminosity Large Hadron Collider HL-LHC. *CERN Yellow Rep.*, (5):1–19, 2015. arXiv: 1705.08830 [physics.acc-ph].
- [15] M. E. Peskin et al. *An Introduction to Quantum Field Theory*. Westview Press, 1995.
- [16] A. Maas. Brout-englert-higgs physics: from foundations to phenomenology. *Progress in Particle and Nuclear Physics*, 106:132–209, 2019. arXiv: 1712.04721 [hep-ph].
- [17] C.-N. Yang et al. Conservation of isotopic spin and isotopic gauge invariance. *Physical Review*, 96(1):191–195, 1954.
- [18] A. Maas. Electroweak physics. Lecture Script. SS 2016. URL: <http://physik.uni-graz.at/~axm/ew2016.pdf> (accessed on: January 23, 2020).
- [19] J. Goldstone. Field theories with superconductor solutions. *Nuovo Cim.*, 19:154–164, 1961.
- [20] M. Böhm et al. *Gauge theories of the strong and electroweak interaction*. Teubner, 2001.
- [21] G. 't Hooft. Renormalizable Lagrangians for Massive Yang-Mills Fields. *Nucl. Phys.*, B35:167–188, 1971.
- [22] V. N. Gribov. Quantization of Nonabelian Gauge Theories. *Nucl. Phys.*, B139:1, 1978.
- [23] I. M. Singer. Some Remarks on the Gribov Ambiguity. *Commun. Math. Phys.*, 60:7–12, 1978.
- [24] E. Seiler. On the higgs-confinement complementarity, 2015. arXiv: 1506.00862 [hep-lat].
- [25] D. Nitz. *Masses of custodial singlet vector particles in Yang-Mills-Higgs theory*. Master’s thesis, University of Graz, Institute of Physics, 2019. URL: <http://physik.uni-graz.at/~axm/theses/nitz.pdf> (accessed on: January 26, 2020).

-
- [26] A. Maas et al. On the phase diagram and the singlet scalar channel in Yang-Mills-Higgs theory. *PoS, LATTICE2014:060*, 2014. arXiv: 1410.7935 [hep-lat].
- [27] F. Knechtli et al. String breaking in SU(2) gauge theory with scalar matter fields. *Phys. Lett.*, B440:345–352, 1998. arXiv: hep-lat/9807022 [hep-lat]. [Erratum: *Phys. Lett.*B454,399(1999)].
- [28] E. H. Fradkin et al. Phase Diagrams of Lattice Gauge Theories with Higgs Fields. *Phys. Rev.*, D19:3682–3697, 1979.
- [29] C. B. Lang et al. The Phase Structure of a Nonabelian Gauge Higgs Field System. *Phys. Lett.*, 104B:294, 1981.
- [30] H. G. Evertz et al. SU(2) Higgs Boson and Vector Boson Masses on the Lattice. *Phys. Lett.*, B171:271–279, 1986.
- [31] A. Maas et al. Spectroscopic analysis of the phase diagram of Yang-Mills-Higgs theory. *Phys. Rev.*, D91(11):113011, 2015. arXiv: 1412.6440 [hep-lat].
- [32] C. Gattringer et al. *Quantum chromodynamics on the lattice*, volume 788. Springer, 2010.
- [33] I. Montvay et al. *Quantum fields on a lattice*. Cambridge Monographs on Mathematical Physics. Cambridge University Press, 1997.
- [34] C. Michael. Adjoint Sources in Lattice Gauge Theory. *Nucl. Phys.*, B259:58–76, 1985.
- [35] S. Prelovsek et al. Scattering phase shift and resonance properties on the lattice: An Introduction. In *Proceedings, Mini-Workshop on Understanding hadronic spectra: Bled, Slovenia, July 3-10, 2011*, pages 73–81, 2011. arXiv: 1110.4520 [hep-ph]. URL: <http://www-f1.ijs.si/Bled2011/book.pdf>.
- [36] C. B. Lang et al. Coupled channel analysis of the rho meson decay in lattice QCD. *Phys. Rev.*, D84(5):054503, 2011. arXiv: 1105.5636 [hep-lat]. [Erratum: *Phys. Rev.*D89,no.5,059903(2014)].
- [37] X. Feng et al. A new moving frame to extract scattering phases in lattice QCD. *PoS, LATTICE2010:104*, 2010. arXiv: 1104.0058 [hep-lat].
- [38] S. Aoki et al. Lattice QCD Calculation of the rho Meson Decay Width. *Phys. Rev.*, D76:094506, 2007. arXiv: 0708.3705 [hep-lat].

- [39] M. Göckeler et al. Scattering phases on finite lattices in the broken phase of the four-dimensional $O(4)$ ϕ^4 theory. *Nucl. Phys.*, B425:413–448, 1994. arXiv: hep-lat/9402011 [hep-lat].
- [40] X. Feng et al. Resonance Parameters of the rho-Meson from Lattice QCD. *Phys. Rev.*, D83:094505, 2011. arXiv: 1011.5288 [hep-lat].
- [41] O. Philipsen et al. On the mass spectrum of the $SU(2)$ Higgs model in $(2+1)$ -dimensions. *Nucl. Phys.*, B469:445–472, 1996. arXiv: hep-lat/9602006 [hep-lat].
- [42] T. A. DeGrand et al. Revealing topological structure in the $SU(2)$ vacuum. *Nucl. Phys.*, B520:301–322, 1998. arXiv: hep-lat/9711032 [hep-lat].
- [43] K. Rummukainen et al. Resonance scattering phase shifts on a nonrest frame lattice. *Nucl. Phys.*, B450:397–436, 1995. arXiv: hep-lat/9503028 [hep-lat].
- [44] T. Yamazaki et al. $I = 2$ $\pi\pi$ scattering phase shift with two flavors of $O(a)$ improved dynamical quarks. *Phys. Rev.*, D70:074513, 2004. arXiv: hep-lat/0402025 [hep-lat].